THE EFFECT OF ANHYDRITE ON ACID FRACTURE CONDUCTIVITY OF A DOLOMITE ROCK

A Thesis

by

DIMAS PERMANA ACHMAD EDHI

Submitted to the Office of Graduate and Professional Studies of
Texas A&M University
in partial fulfillment of the requirements for the degree of

MASTER OF SCIENCE

Chair of Committee,	A. Daniel Hill
Committee Members,	Ding Zhu
	Yuefeng Sun
Head of Department,	Jeffrey B. Spath

December 2019

Major Subject: Petroleum Engineering

ABSTRACT

In this study, we conducted laboratory experiments of acid fracturing using San Andres dolomite downhole sample cores and regular HCl acid 15%. These samples have variation of anhydrite content from 1% to 43% based on XRPD analysis and three different types of anhydrite's distribution. In the experiments, we used treatment conditions that represented field and reservoir condition. Besides, acid etched volume and acid fracture conductivity at different closure stress were measured and calculated using surface scan profilometer and conductivity measurement apparatus consisting of modified API conductivity cell and loading frame, respectively. Acid fracture conductivity decline was evaluated and compared to the three different type of anhydrite distribution. Also, acid fracture conductivity at closure stress 0 psi and 3,000 psi were evaluated to see the correlations of acid fracture conductivity to the percentage of mineralogy of anhydrite and dolomite. In addition to that, acid fracture conductivity was compared to other carbonate rocks such as limestone and chalk. Therefore, this study aims to study the effect of anhydrite distribution on the fracture surfaces of a dolomite reservoir to acid fracture conductivity.

Based on experimental results, acid fracture conductivity decline and initial acid fracture conductivity at 0 closure stress showed that there were three different acid fracture conductivity decline and initial conductivity at 0 closure stress which could be grouped based on three different types of anhydrite distribution. Patchy distribution showed high initial conductivity and high conductivity decline rate, pore-filled distribution showed

moderate initial conductivity and moderate conductivity decline rate, and bedded distribution showed low initial conductivity and low conductivity decline rate because the direction of bedded distribution is perpendicular to the fluid flow considering the way coring was carried out.

Based on graphical plots of acid etched volume and acid fracture conductivity, these plots showed poor correlation of acid etched volume and acid fracture conductivity to the percentage of mineralogy, which is anhydrite and dolomite. However, removing outlier and samples that have non-anhydrite greater than 2%, these plots showed good correlations that acid etched volume and acid fracture conductivity are proportional to the percentage of dolomite but both parameters are inversely proportional to the percentage of anhydrite. The conclusion of the study is that anhydrite presence in the dolomite reservoir is affecting to the value of acid fracture conductivity at the initial and at the selected closure stress and also affecting to the declining rate of acid fracture conductivity.

DEDICATION

This work is dedicated to my parents, my love – Mutia, and my children – Faris, Adib and Zidan for their unconditional love and support during the good and the bad times.

ACKNOWLEDGEMENTS

I would like to thank Dr. A. Daniel Hill and Dr. Ding Zhu who patiently guided and supported me throughout the course of this research. I also would like to acknowledge Dr. Yuefeng Sun for serving as committee member.

I would like to thank,

- Xiao "Jimmy" Jin who helped me complete the experimental work from the beginning to the end.
- John Maldonado who helped me provide any assistance with acid disposal and equipment's problem
- Joevan Beladi who helped me cut out core sample for preparing XRPD samples
- Igor Ivanishin who helped me run XRPD for all samples
- Gabriel Tatman who helped me crush the rock for some of XRPD samples
- My friends, colleagues and the department faculty and staff who made my time at Texas A&M University a great experience
- My parents, my love - Mutia, and my children (Faris, Adib, and Zidan) for their continuous and unconditional support.

Finally, thanks to LPDP (Lembaga Pengelola Dana Pendidikan)/ Indonesia Endowment Fund for Education for sponsoring my master program and ASRP (Acid Stimulation Research Program) for funding the research project.

CONTRIBUTORS AND FUNDING SOURCES

Contributors

This work was supervised by a thesis committee consisting of Professor A. Daniel Hill [committee chair], Professor Ding Zhu [committee member] of the Department of Petroleum Engineering and Professor Yuefeng Sun [committee member] of the Department of Geophysics and Geology.

The experimental work for Chapter 2 was assisted by Xiao “Jimmy” Jin, Igor Ivanishin, John Maldonado, and Joevan Beladi of the Department of Petroleum Engineering. All other work conducted for the thesis was completed by the student independently.

Funding Sources

Graduate study was supported by Indonesia Endowment Fund for Education (LPDP) and thesis research was supported by Acid Stimulation Research Program (ASRP).

NOMENCLATURE

Acronyms

XRPD	X-Ray Powder Diffraction

Variables

$k_f w$	Fracture Conductivity, md-ft
w	Fracture Width, in
q	Flow Rate, ltr/s
ρ	Density, lb/ft^3 or kg/m^3 or gr/cc
μ	Viscosity, cP or Pa-s
M	Molecular Mass, kg/kg-mol
Z	Gas Compressibility Factor
R	Universal Gas Constant
P	Pressure, psi
h	Fracture Height, in

TABLE OF CONTENTS

Page

LIST OF FIGURES

Page

LIST OF TABLES

Page

1. INTRODUCTION

1.1. Carbonate Reservoirs

Carbonate reservoirs are well-known as reservoir with complex problems. Carbonate mineral system is relatively simple because it is dominated by calcite, aragonite, Mg-calcite and dolomite. All of them are relatively soluble and therefore susceptible to dissolution, even in the same environment where they formed. Hence lie the complexities of carbonate reservoirs (James et al 2016).

Carbonate rocks are significantly different from siliciclastic rocks. Siliciclastic rocks are composed of a variety of silica-based grains that may have traveled hundreds of miles from their source, while carbonate rocks mainly consist of two minerals, which are calcite and dolomite, and remain near their point of origin (Akbar et al 1995).

Siliciclastic rocks are mostly dominated by sandstones and shales that contain a wide variety of minerals and particles, such as quartz, oligoclase feldspar, clay minerals, and fragments of preexisting rocks and remnants of plants or animals. On the other hand, carbonate rocks consist of a more limited group of minerals, which are calcite and dolomite, even though other minerals may be present in the carbonate rocks such as anhydrite, gypsum, quartz, clay minerals, pyrite, ankerite, and siderite (Akbar et al 2001). The presence of other minerals in the reservoir increases the complexities of carbonate reservoir since the other minerals have different behavior from the main carbonate minerals.

These distinctions cause significant differences in classifying and evaluating between siliciclastic rocks and carbonate rocks, with siliciclastic rocks characterized by

grain composition and size, and carbonate rocks distinguished by depositional texture, grain or pore types, rock fabric or diagenesis.

1.2. Dolomite

The difficulty in classifying carbonates to reflect both their current state and depositional history demonstrates how dominant diagenesis is in forming the final carbonate rock.

In carbonate, once deposited, sediments undergo diagenesis, the post depositional chemical and physical changes that transform the sediment into solid rock. Carbonate diagenesis can significantly modify pore space and permeability. Carbonate rocks are so susceptible to dissolution that grains can be dissolved to form new pore space, and dissolution along fractures and bedding planes can produce large vugs and caves. Meanwhile, clastic diagenesis normally does not involve a change in mineralogy.

Carbonate diagenesis commonly involves replacing partly or wholly of the original calcite with the mineral dolomite in a variety of ways and can happen at any time in the history of deposition, called dolomitization and modify the hydrocarbon-producing characteristics.

Dolomite is precipitated in shallow sediments on the seafloor and in marginal marine environments and it replaces carbonates in contact with shallow ground-water during deep burial and from hydrothermal fluids. Dolomite replacement of calcite is generally expressed in the equation 1.

$$2CaCO_3 + Mg^{2+} \rightleftharpoons CaMg(CO_3)_2 + Ca^{2+} \quad (1)$$

1.3. Anhydrite

Anhydrite ($CaSO_4$) and gypsum ($CaSO_4.2H_2O$) are evaporate minerals that may be present in carbonate rocks and are commonly found in dolomite reservoirs. Gypsum is the common evaporate mineral found in modern sediments and at shallow depths. The change from gypsum to anhydrite is controlled by temperature and the activity of water. The increase in temperature with depth results in near-surface gypsum converting to anhydrite (Lucia 1999).

There are four type of anhydrite commonly found in dolomite rocks (Lucia 1999):

1. Poikilotopic

   It is large crystals of anhydrite with inclusions of dolomite and is often distributed randomly throughout the rock. It is typically scattered and unevenly distributed as depicted in the Figure 1.

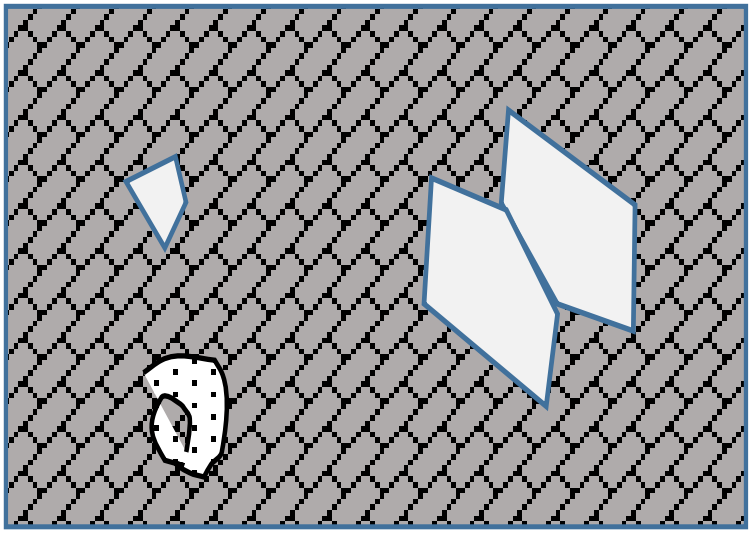

Figure 1 Poikilotopic (Adapted from Lucia 1999)

2. Nodular

It is found in dolostone in the form of microcrystalline masses of anhydrite, as depicted in Figure 2, and commonly forms within the sediment by displacement as either anhydrite or gypsum.

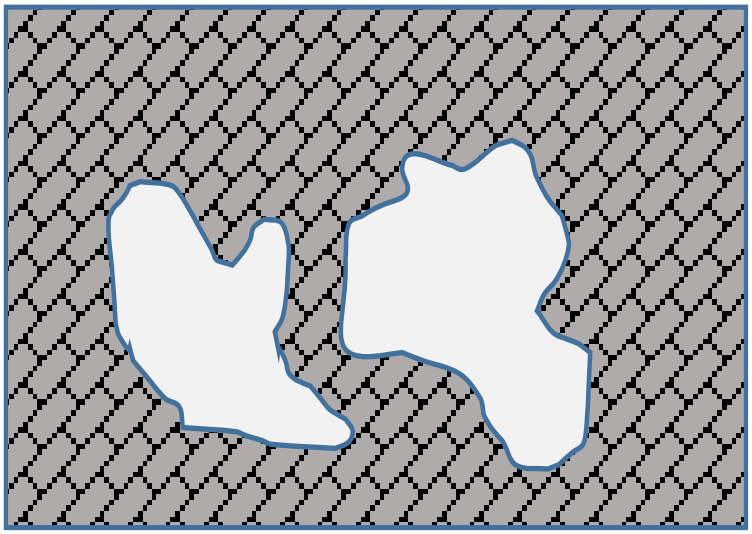

Figure 2 Nodular (Adapted from Lucia 1999)

3. Pore-filled

It is typically pervasive and reduces both porosity and pore size distribution of carbonate reservoir rocks, as shown in the Figure 3, because it occludes inter-grain, inter-crystal, and vuggy pore space.

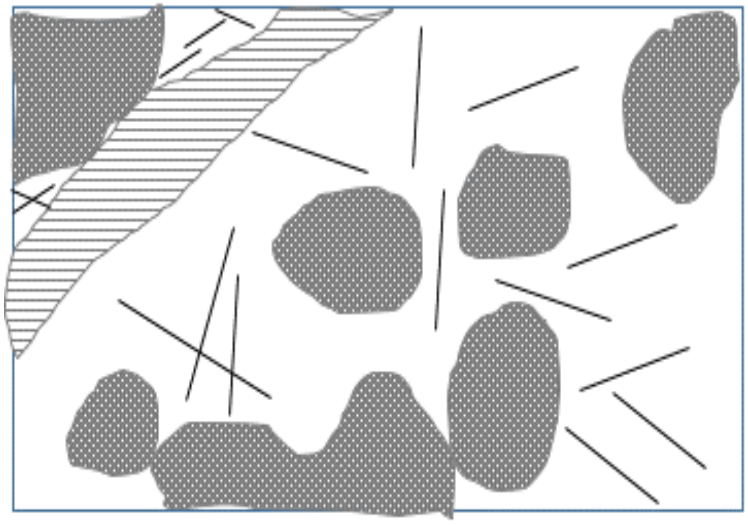

Figure 3 Pore-filled (Adapted from Lucia 1999)

4. Bedded Anhydrite

It is found in laterally continuous beds a few inches to hundreds of feet thick and is deposited out of a hypersaline body of water as gypsum and later is converted to anhydrite. It can be either laminated or composed of coalesced nodules as shown in the Figure 4. The coalesced nodules may form by precipitation out of a body of water as gypsum or by displacement and replacement of near-surface sediment as either gypsum or anhydrite.

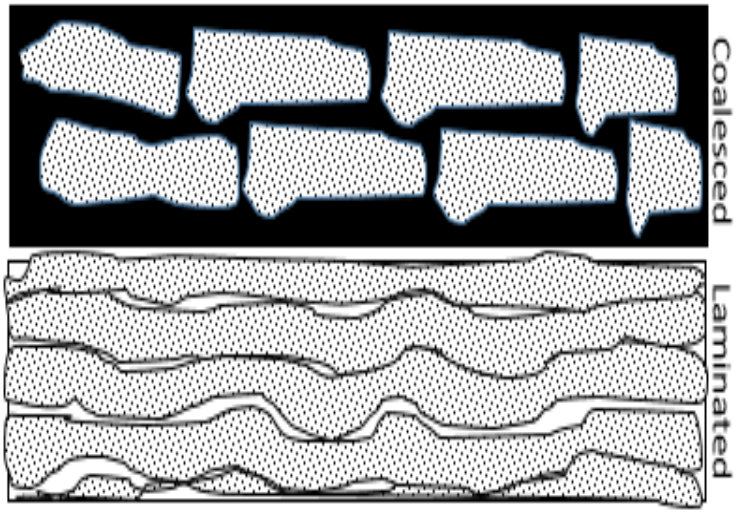

Figure 4 Bedded anhydrite (Adapted from Lucia 1999)

However, based on its distribution, anhydrite can be divided into three types of distribution, which are patchy distribution (poikilotopic and nodular), pore-filled (even distribution), and laterally continuous (bedded).

Diagenetic gypsum and anhydrite are commonly associated with dolomitization and require the transport of sulfate into the system by high sulfate and hypersaline water. Studies have shown little linkage between depositional facies patterns and patterns of diagenetic gypsum or anhydrite. This increases the complexities of dolomite rocks that have anhydrite or gypsum presence.

1.4. Acid Fracturing

Acid fracturing is well stimulation technique that is commonly performed to improve well productivity or injectivity from carbonate reservoir and achieve the objective of bypassing formation damage and stimulating undamaged formation (Kalfayan 2007). In acid fracturing, acid is injected at pressures above fracturing pressure using high

viscosity fluid as a pad to create fracture. The viscous fluid as a pad can be acid itself or non-reactive cross-linked water. Following this viscous fluid to create a fracture, acid, which can be plain acid (HCl), gelled-acid, foamed-acid, or an emulsion acid, is injected into the created fracture to dissolve rock minerals and create differential etching that will act as pillars and provide conductive path for fluids to flow when the created fracture closed after injection stops.

In carbonate reservoirs where it has high degree of complexities because of high degree of heterogeneity, this complex heterogeneity has significant role since it can affect etching pattern, etching volume and an aperture which will eventually determine the acid fracture conductivity. In addition to that, type of carbonate reservoirs also influences the result of acid fracture conductivity. Based on experimental work performed by Lund et al (1973) and confirmed by Taylor et al (2004), calcite ($CaCO_3$) has higher dissolution rate than dolomite ($CaMg(CO_3)_2$) as depicted in the Figure 5. This fact triggers the question whether dolomite is good candidate for acid fracturing because its dissolution rate is 10 times lower than calcite and increases the complexities of managing dolomite reservoirs.

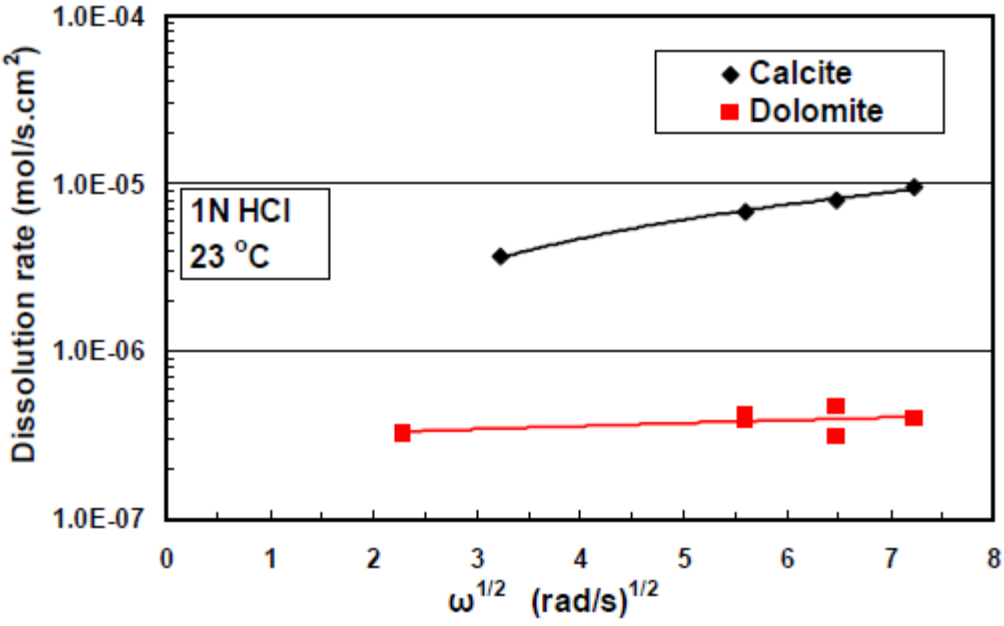

Figure 5 Dissolution rate comparison between calcite and dolomite (Reprinted from Taylor et al 2004)

The chemical reaction between HCl and calcite and HCl and dolomite are written as follows:

1. Calcite:

$$2HCl + CaCO_3 \rightarrow CaCl_2 + CO_2 + H_2O \quad (2)$$

2. Dolomite:

$$4HCl + CaMg(CO_3)_2 \rightarrow CaCl_2 + MgCl_2 + 2CO_2 + 2H_2O \quad (3)$$

Besides, other parameters are affecting the result of acid fracturing such as temperature, pressure, acid type, acid concentration, acid velocity, reaction products, and formation heterogeneity.

In acid fracturing, acid fracture conductivity is the measurement of flow capacity through the acidized fracture. This is the important parameter that is usually compared

when other operational and design parameters are evaluated to find the optimum condition. Acid fracture conductivity is not only affected by etching pattern and etching volume but also the strengths of the pillars that keep the fracture open and the amount of closure stress on the fracture after injection stopped. Thus, acid fracture conductivity is difficult to predict and, currently, the way to predict it has been using empirical correlation developed by Nierode – Kruk (1973) or Mou – Deng (2012).

There have been many experimental works in acid fracturing to understand how operational and design parameters affect the acid fracture conductivity using different type of experimental methods. These experimental works continuously develop and improve our understanding of acid fracture conductivity and its affecting parameters. Based on these experimental works as well, empirical correlation of determining acid fracture conductivity was developed.

Barron et al (1962) studied the relationship between reaction rate of HCl acid and its shear rate. They estimated the spending time and penetration distance of an acid in a fracture and also developed an equation relating injection rate, fracture width, acid concentration, contact time, and fracture height for both linear and radial fracture systems. They concluded that the time spent by acid in a fracture depends on the reaction rate, which depends on temperature, pressure, rock composition, and the ratio of the acid volume to the surface area of the rock.

Broaddus et al (1968) studied the effect of acid type, temperature, and contact time on the resultant fracture conductivity. They found that acid fracturing of limestone with straight HCl at lower temperatures (80 – 150 F) produced higher conductivity than the test

with retarded acid. The results were opposite for acid fracturing performed with two types of acids at higher temperatures. Also, it showed that the increase of contact time may improve the fracture conductivity in some cases. However, over-etching could also happen resulting in rock crushing under closure stress and have low acid fracture conductivity that concluded the maximum acid fracture conductivity could be achieved at the optimum etching conditions.

Nierode and Kruk (1973) conducted experiments using core plugs that had 1 in. diameter and 2 – 3 in. long, with rough fracture surfaces and no fluid loss. After injection of acid emulsions and viscous acids, they found that conductivity occurred because some peaks and valleys of fracture face were smoothed due to acid dissolution and creating an aperture after applying closure pressure. They also developed empirical correlations to determine acid fracture conductivity that has been widely used in the industry.

Anderson and Fredrickson (1989) developed a laboratory procedure to measure acid fracturing conductivity of cores in order to optimize treatment parameters. They confirmed that etching volume affecting fracture conductivity depends on treatment parameters, such as acid type and concentration, reaction time, temperature and flow regime.

Malik and Hill (1989) studied the effect of acid leak-off into the formation on acid fracture conductivity. The study showed that acid fracture conductivity on limestone sample, which was injected using acid with and without leak-off, was quite similar except significant decline was observed without leak-off at high closure stress.

Bartko et al (1992) carried out an experiment to study the effect of different acid type on acid fracturing conductivity for limestone and dolomite. The study showed that 15% emulsified acid type had the lower acid fracture conductivity than 10% emulsified acid type, which was probably caused by the weakening effect happened to rock treated with 15% emulsified acid type.

Van Domelen (1992) studied the influence of acid spending and leak-off of reactive fluids to predict etched fracture conductivity and effective fracture length. The study showed that surface reaction rate of many formations is lower than the rate predicted from laboratory and concluded that fluid leak-off is the primary cause that limits effective fracture length and fluid loss coefficient is related to initial permeability.

Van Domelen (1994) conducted another experiment to study the reactivity of the formation and characterize etching characteristics. The result showed that relative difference between zero-closure stress conductivity and conductivities at higher closure stress provides quantitative estimation of the degree of differential etching.

Beg et al (1996) studied the effect of contact time and fluid loss on acid fracture conductivity for different types of rocks. The study showed that experiments with leak-off tend to have higher acid fracture conductivity than without leak-off. Besides, acid fracture conductivity for experiments with longer contact time resulted in lower conductivity because of weakening effect of acid fracture face. These results indicated that there should be optimum contact time that can have adequate etching dissolution to produce higher acid fracture conductivity, which is in the middle of too much dissolution causing weakening

effect and too little dissolution causing no differential etching and aperture on the fracture face.

Gong et al (1998) studied the effect of contact time and acid leak-off on acid fracture conductivity. The results were that the longer contact times, the wider of asperities' growth of height distribution and the rougher fracture surface, the higher acid fracture conductivity. Besides, results showed that acidized fracture face had lower value of hardness number than non-acidized fracture face.

Abass et al (2006) studied the effect that elastic, plastic, and creeping deformations have in reducing fracture conductivity. The experiments focused on the rock mechanics aspect of fracture closure, and applying creeping test to provide an additional criterion for use in selecting between proppant and acid-fracturing. The study concluded that the well productivity decreases in acid fractured well is an integrated effect of elastic, plastic, and creeping responses to applied closure stress.

Melendez (2007) studied the effect of rock hardness variation and surface etching on acid fracture conductivity. The study carried out experiments using polymer gelled-acid into different rock types (limestone, dolomite, and chalk) with variation in injection times. In this study, rock hardness was measured before and after injection and compared to acid fracture conductivity. This study showed that acid fracturing conductivity is not only governed by etching pattern of the rock surface but also influenced by the hardness of the rock. If there is a channel created after injection, this channel provides a conductive path for fluid to flow. However, if there is no channel created after injection, rock hardness plays important role to provide conductivity. The effect of hardness variation on acid

fracture conductivity are higher in dolomite than limestone and chalk. Lastly, the study showed that longer contact times and higher etched volume do not always mean high acid fracture conductivity.

Malagon (2007) studied the acidized fracture surface by developing a device called surface scan profilometer using laser to improve the understanding of remaining etched surface topography, hydro-dynamics effect and calculating acid etched volume by comparing before and after acid dissolution. The study showed that the effect of dissolution depends on the type of rock and the fluid system.

Pournik et al (2008) studied the effect of treatment conditions on etching, rock weakening, and resulting acid fracture conductivity that would be used to develop design criteria for acid fracturing treatments.

Antelo et al (2009) studied that acid fracture conductivity is a function of the amount of rock dissolved, which is controlled by kinetic parameters and the mineralogical composition along with the degree heterogeneity of the rock.

Neumann et al (a.2012) studied the feasibility of acid fracturing on hard-and-deep limestone reservoirs. This study concluded that acid fractures can exist in carbonate reservoirs with closure stress greater than 5,000 psi. In another study, Neumann et al (b.2012) showed the difference between sample rocks with wet sawed fracture faces and tensile fracture surfaces. The study concluded that surface of tensile fractures after acid etching can be smoother, rougher, or remain the same.

Penaloza et al (2013) investigated the effect of temperature, rock-acid contact time, and initial condition of the fracture surfaces on acid fracture conductivity for Austin Chalk

formation. The results showed that there was no significant difference in acid fracture conductivity at high closure stress using either smooth or rough fracture surfaces.

Almomen (2013) studied the effect of initial condition of fracture surfaces on the etching pattern and acid fracture conductivity, the variation of acid fracture conductivity along the fracture due to acid spending, and the effect of contact time, acid systems, and temperature effects on acid fracture conductivity using San Andres dolomite formation. The results showed that rough surfaces have higher acid fracture conductivity at low closure stress than smooth surfaces, increasing of acid spending did not result in lower acid fracture conductivity and acid etched volume itself was not sufficient to predict acid fracture conductivity because acid fracture conductivity is affected by etching pattern, etching volume and rock compressive strength. Besides, based on acid fracture conductivity, linear-gelled acid resulted in higher acid fracture conductivity at higher temperatures while in-situ cross-linked acid resulted in higher acid fracture conductivity at lower temperatures.

Underwood (2013) studied the effectiveness of 15% HCl as stimulation fluid for acid fracturing using core samples from a limestone reservoir. The experiment used six core samples and resulted that acid fracture conductivity had the most impact on core samples that have higher acid solubility greater than 50% and not recommended for the one that has less than 50% acid solubility.

Suleimenova (2015) investigated the effect of rock lithology, porosity, and permeability on the acid fracture conductivity for the Middle Canyon formation using six downhole core samples taken from different depth. The results showed that acid fracture

conductivity at 4,000 psi was similar for all sample cores regardless variation of rock properties and acid fracture conductivity for lower porosity samples had lower decline rate of conductivity.

Wang (2015) evaluated the factors that affect the efficiency of acid fracturing for heterogeneous carbonate formation and compared conductivity for unpropped, propped-fracture, and acid fracture. The results showed that propped-fracture was better than acid fracture and unpropped especially at high closure stress. Fracture surface channels created by acid could help to improve acid fracture conductivity at lower closure stress. However, as closure stress increases, the strength of surface rock starts to dominate acid fracture conductivity.

Jin (2019) studied the effect of heterogeneity and distribution of insoluble mineral on acid fracture conductivity by carrying out experimental works using homogeneous limestone from the outcrop and heterogeneous limestone core samples from downhole cores. He also carried out XRD and XRF to identify the distribution of mineral on the fracture surfaces. The results showed that insoluble minerals with higher mechanical properties were not crushed at high closure stress and had shallower acid fracture conductivity decline rate. If the acid etching creates sufficient acid etched volume, rock sample could sustain conductivity at higher closure stress.

Nevertheless, there were no study investigating the effect of anhydrite, which is commonly found in the carbonate reservoirs especially dolomite reservoirs, on the fracture surfaces. Therefore, a study to investigate the effect of anhydrite on acid fracture

conductivity of dolomite rocks is required to improve our understanding of acid fracture conductivity.

1.5. Research Objective

This research aims to investigate the effect of anhydrite as insoluble material in dolomite reservoirs and its distribution on the fracture surfaces to the acid fracture conductivity using downhole San Andres dolomite sample cores which have variation of anhydrite content in downhole sample cores. Besides, it also aims to investigate whether dolomite rock, which have anhydrite distribution on the fracture surfaces, is still a good candidate for acid fracturing by comparing with acid fracture conductivity from other rock types' experimental results.

2. EXPERIMENTAL SET UP, TESTING CONDITIONS, AND PROCEDURE

2.1. Experimental Set Up and Testing Conditions

In this experimental study, there were several different experimental works carried out to complete the study, which were as follows:

1. Core Sample preparation
2. Fracture Surface Characterization
3. Acid Injection
4. Conductivity Measurement

These experimental works were designed to properly scale and represent field condition.

This experimental study used field core samples taken from three different wells at different depth of San Andres dolomite formation, as shown in the Table 1. These wells are located in two different counties in the West Texas, as shown in the Figure 6.

Table 1 Well information

#	Well Name	API #	Interval, ft		County
			Top	Bottom	
1	Higginbotham #1	42-501-32807	5218.4	5270.5	YOAKUM
2	North Lawson #5-12	42-135-33927	4302.5	4339.7	ECTOR
3	North Lawson #13-4	42-135-34109	4338	4378	ECTOR

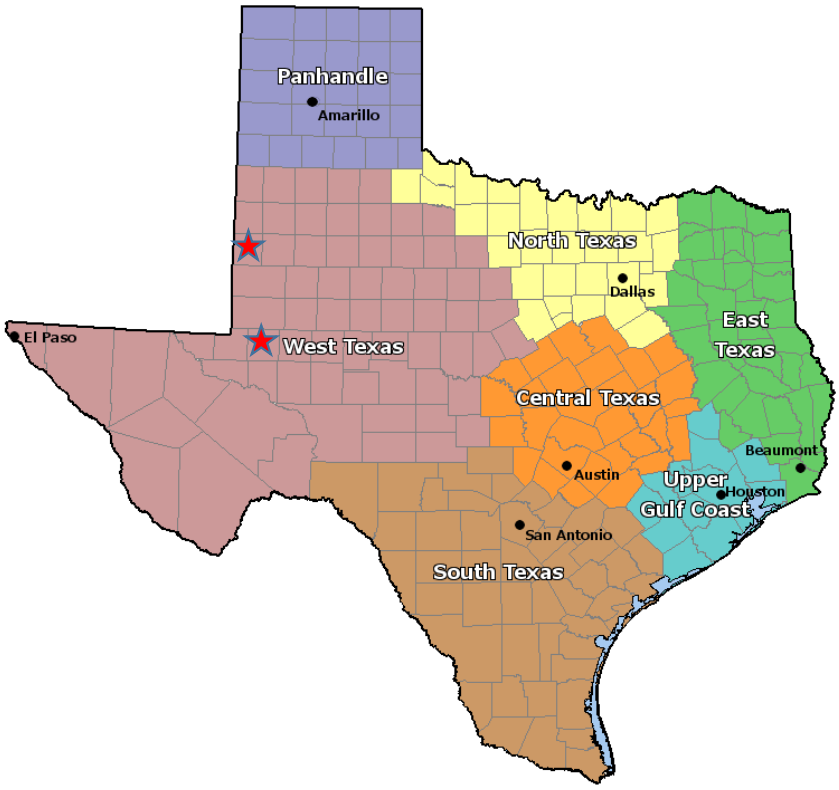

Figure 6 Well's location in the two different counties in West Texas

These San Andres dolomite rock samples were selected from series of slab cores and cut to specific shape and size. The shape used in this study was rectangular with rounded edges and the sample had dimension of 7.25-in length, 1.75-in width, and 3-in height. Then, these rock samples were loaded with tensile stress to break the rock samples into two halves (approximately 1.5-in height) and make a rough surface on rock samples. After that, these rock samples were covered by silicone-based sealant inside the mold so that they could be perfectly inserted into the acid injection cell. Prior to inserting in to the acid injection cell, these samples were scanned using a laser profilometer to capture the topography of fracture surface as a base-case that would be compared with condition after

acid injection to see how much minerals were dissolved by HCl acid and calculate acid etched volume.

Acid injection cell was made of Hastelloy C-276 material which was resistant to acid corrosion. Besides, it was a modified API cell RP-61which could accommodate larger core samples. This cell was equipped with two side pistons and marked its flow direction and core samples covered by silicone-based sealant and given its dimensions are shown in the Figure 7.

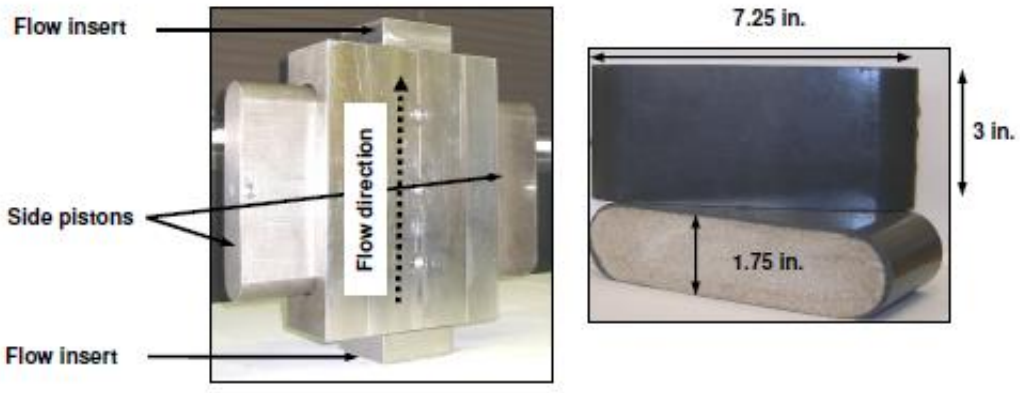

Figure 7 Modified API cell RP-61 and sample dimension (Reprinted from Melendez 2007)

Core samples were then inserted in to acid injection cell from right and left side, left with a gap 0.12 inches to represent fracture in the middle of both rough surfaces. The core samples inside the cell were sealed by side pistons to hold the samples inside the cell while applying pressure during fluid injection. The side piston at the right and left side were equipped with predefined channel mold on its face and flow connection on its back to allow leak-off mode in this experiment. The fluid flowed through 0.12 inches gap in the

middle of the cell from flow insert at the bottom to the top. The schematic of acid injection experiments is depicted in Figure 8.

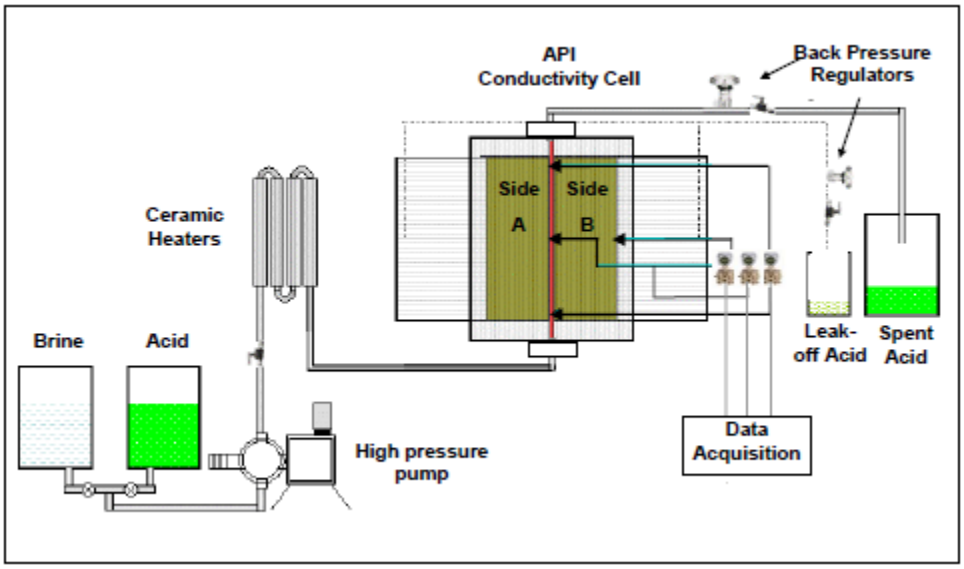

Figure 8 Acid injection apparatus (Reprinted from Melendez 2007)

In this experiment, water was initially pumped to ensure the system connections well-connected and set up. While pumping the water, ceramic heaters and a heating jacket were used to increase temperature on the fluid flow and injection cell to the desired condition. In this experiment, desired conditions were 130 ºF temperature, 1,000 psi pressure, 1 L/ min injection flow rate, and 10-minute injection time. Once the desired conditions were achieved, water was switched to acid injection. The pressure was kept at around 1,000 psi by controlling a backpressure regulator in order to maintain CO_2 gas in solution. Leak-off fluid was controlled through the use of a backpressure regulator in the leak-off line. Spent acid and leak-off fluids were collected in the different containers.

There were three different pressure transducers, which were used to monitor pressure conditions in the system.

After acid injection, core samples were scanned with the laser profilometer for post injection condition. Then, both samples were put together on its faces that were leaving some apertures due to acid etching. Silicone-based sealant was used to cover both samples together and ready for fracture conductivity measurement. Acid fracture conductivity was measured under step-changed closure stress to represent actual condition when injection stopped. In the experiment, closure stress was produced with the load frame CT-250. Closure stress applied in the experiment were from 1,000 psi to 8,000 psi with incremental changes of 1,000 psi. Acid fracture conductivity was measured by flowing nitrogen through the middle of the fracture surfaces of the core samples inside conductivity cell and recording four different flow rates, differential pressure, and cell pressure for each closure stress and calculating it using Darcy's equation. Schematic of acid fracture conductivity could be seen in the Figure 9.

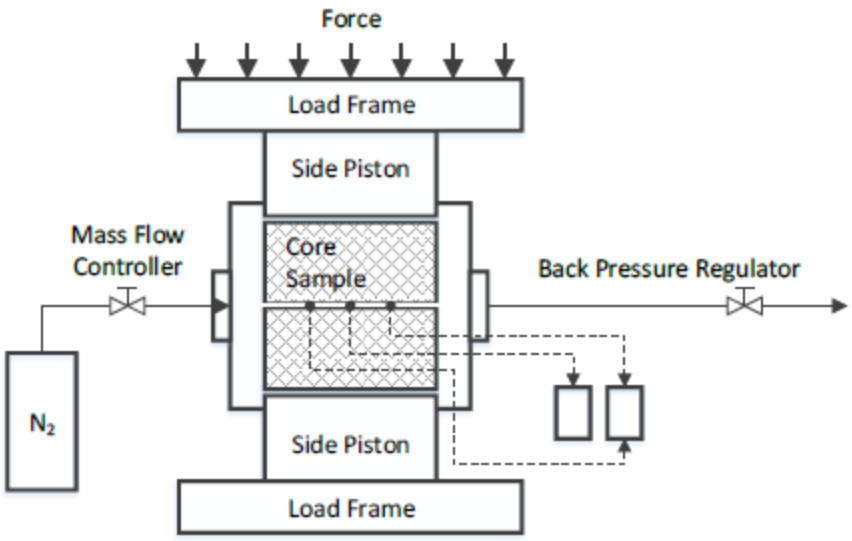

Figure 9 Acid fracture conductivity apparatus (Reprinted from Suleimenova 2015)

2.2. Core Sample Preparation

This was the first step of the experimental study, which was preparing core samples. There were 12 pairs of dolomite core samples used in these experiments. The objective of core samples preparation was to make sure that core samples were perfectly fitted and inserted into the acid injection cell and conductivity cell. Besides, the perfect fit into the cell was required to avoid any leaking from injection fluid either water, acid or gas because if any leaking occurred during the experiment, it would mislead the result and analysis of the experiment.

There were two types of sample core preparations based on the type of experiments. The first one was acid injection experiment and the second one was acid fracture conductivity measurement, as shown in the Figure 10 and Figure 11, respectively.

The steps below explained the detailed procedure of core sample preparation for acid injection experiment:

1. Clean the fracture surface of core samples from dust generated from cutting process. Mark the bottom of core samples with sample number and flow direction to make sure that all flow directions for each core samples are consistent along the experimental works.
2. Create composite core as a spacer with the same dimension as the dolomite core samples, but with half of the height (1.5-in), to make up core samples to have around 3-in height.
3. Apply tape to the top of spacer and the bottom of dolomite core samples, the upper part of dolomite core samples, and the bottom of spacer to protect the top and bottom of dolomite core samples and spacers from silicone contamination that will affect the dissolution of acid on fracture surfaces and prevent acid leak-off flow through dolomite core samples to spacer and side pistons.
4. Apply silicone primer (SS4155) on the side walls of the cores and wait for 15 minutes until it is dry. Then, repeat this step for three times.
5. Clean metal surface of the small mold. Apply silicon release spray and wait for 5 minutes. Then, repeat this step for three times.
6. Assemble the mold and screw on four bottom and three side screws.
7. Put core samples into the mold and adjust to center position.

8. Mix one part of silicone potting compound with one part of silicone curing agent using the ratio of 1:1 by weight (55 gr : 55 gr) and stir the mixture well to obtain homogeneous grey-colored liquid.
9. Pour the mixture into the clearance between core samples and mold.
10. Leave the sample for 30 minutes to make sure that there are no bubbles in the mixture and in the clearance between core samples and mold.
11. Put the mold and core samples into the laboratory oven and set temperature to 60 – 80 C and leave it in the oven for three hours.
12. Remove the mold from the oven and let it cool down for 1 hour.
13. Remove the screws on the mold (under and side of the mold), disassemble the mold and carefully take out the core samples from the mold.
14. Cut the silicone at the edges of the core surfaces and match the edges of the core to the fracture surfaces if possible.

Besides, there was also core sample preparation for fracture conductivity measurement, which was a similar but shorter procedure than preparing core samples for acid injection. The steps below explain the detailed procedure of core sample preparation for fracture conductivity measurement:

1. Clean the fracture surface from any acid or water from acid injection and apply glue to the bottom of dolomite core samples and top of spacers and tape to the middle of fracture surfaces.
2. Apply silicone primer (SS4155) on the side walls of the cores and wait for 15 minutes until it is dry. Then, repeat this step for three times.

3. Clean the metal surface of the large mold. Apply silicon release spray and wait for 5 minutes. Then, repeat this step for three times.
4. Assemble the mold and screw on four bottom and three side screws.
5. Put core samples into the mold and adjust to center position.
6. Mix one part of silicone potting compound with one part of silicone curing agent using the ratio of 1:1 by weight (110 gr : 110 gr) and stir the mixture well to obtain homogeneous grey-colored liquid.
7. Pour the mixture into the clearance between core samples and mold.
8. Leave the sample for 30 minutes to make sure that there are no bubbles in the mixture and in the clearance between core samples and mold.
9. Put the mold and core samples into the laboratory oven and set the temperature to 60 – 80 ºC and leave it in the oven for three hours.
10. Remove the mold from the oven and let it cool down for 1 hour.
11. Remove the screws on the mold (under and side of the mold), disassemble the mold and carefully take out core samples from the mold.
12. Cut the silicone at the edges of the core surfaces, match the edges of the core to the fracture surfaces if possible, create a hole at the inlet, outlet, and three points at pressure transducer positions.

Figure 10 Rock sample preparation for acid injection experiment

Figure 11 Rock sample preparation for acid fracture conductivity measurement (Reprinted from Jin 2019)

2.3. Fracture Surface Characterization

The profilometer scanner is a precise vertical distance measurement device that can measure small surface variations in vertical surface topography as a function of the sample position, as shown in Figure 12. The vertical measurement is made with a laser displacement sensor while core samples are moving along its length on a moving table. That measurement is repeated several times over the width of the sample to cover the entire surface area. This profilometer is used to measure the topography of fracture surfaces and characterize core samples before and after acid injection. Besides, this profilometer is also used to calculate acid etched volume that represents how much volume of mineral was dissolved by acid.

The steps below explain the detailed procedure of profilometer scanner for surface characterization:

1. Place the rock sample on the table and secure it using table screws.
2. Adjust the laser sensor using the vertical milling table screw to ensure full range measurements over the surface topography. Guidelines for adjusting the vertical milling table are as follows:
    a. Ensure that top of the fracture surfaces have more than 0.8 inches but less than 1.8 inches from laser scanner (0.8 inches < top fracture surface < 1.8 inches). 1-inch range in this step is range that can be read by the laser scanner.

b. Ensure that the value of z at several points from highest point of the fracture surfaces (at the top) to the lowest point of the fracture surfaces show real value of vertical measurement, not just default value.

3. Set the X and Y distance indicators to zero manually using the control box front panel.
4. Switch the control panel to automatic on the control box, as shown in Figure 13.
5. Input the data file location, experimental information, and sample dimensions on the pop-up software user window.
6. Start scanning by clicking on the start button on the software screen and let the scanning process run for three to four hours.
7. Use the Matlab program to process the image and calculate acid etched volume.

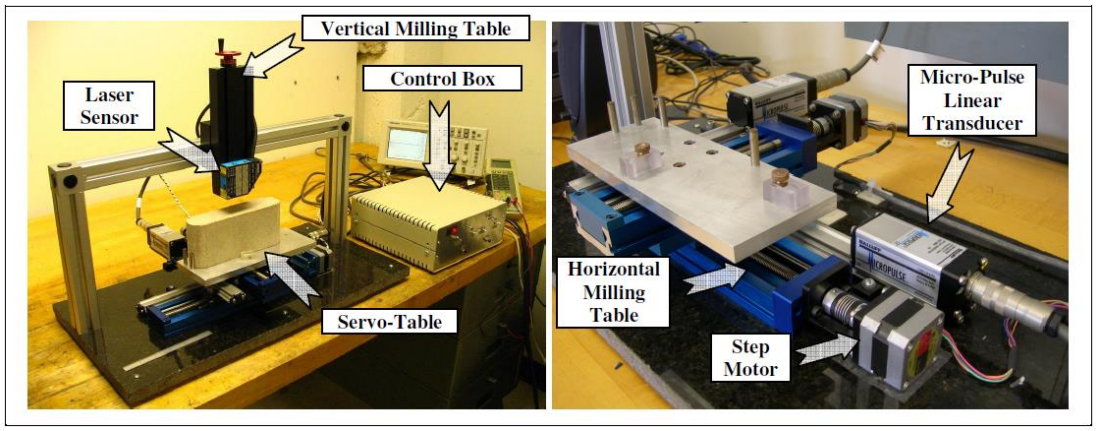

Figure 12 Surface scan profilometer equipment (Reprinted from Malagon 2007)

Figure 13 Control panel of surface scan profilometer (Reprinted from Malagon 2007)

2.4. Acid Injection Experimental Procedures

In this experimental work, core samples are etched with the acid system under certain conditions of contact time, pumping rate and temperature. In this experiment, desired conditions were 130 ºF temperature, 1,000 psi pressure, 1 L/min injection flow rate, and 10-minute injection time. The steps below explain the detailed procedure of an acid injection experiment:

1. Saturate core samples with water by using the glass vessel with a lid connected to the vacuum pump, as shown in the Figure 14.

2. Remove the core samples and let them dry. Apply thin layer of grease on the side of the cores to make it easier to be inserted in to the acid injection cell.
3. Insert the sample cores to the acid injection cell from left and right side, make sure that both fracture surfaces meet in the middle of acid injection cell, and use shim to provide gap 0.12 inch in the middle and between fracture surfaces of core samples as a width of fracture.
4. Insert the pistons into the cell and push them inside using hydraulic jack until they touch the core samples. Use a shim and place in between fracture surfaces to make sure when the piston is pushed using hydraulic jack, there is still a gap in the middle of fracture surfaces.
5. Assemble the remaining acid injection cell and connect all lines from the pump, acid injection cell, and fluid collector and make sure that hydraulic jack is locked to prevent movement during injection process as depicted in the Figure 15.
6. Connect the thermocouple in the inlet and outlet lines. In the inlet line, connect the thermocouple to the portable thermometer. In the outlet line, connect the thermocouple to the temperature controller.
7. Cover the cell with the heating jacket and connect it to the temperature controller. Set up the temperature of the heating jacket to 130 F. Pre-heat the cell for 1 – 2 hours before acid injection.
8. Prepare 15% HCl by mixing 28% HCl with water under the fume hood.

9. Start magnetic stirring to continuously stir the mixing-fluid of 15% HCl during the experiment.
10. Start the pump by pumping water. Check all connections and ensure that there is no leakage. If there is a leakage, fix it immediately. Measure the flow rate and ensure that flow rate is 1 L/min.
11. Set the cell pressure 1,000 psi by gradually increasing the pressure. Make sure that the leak-off port is functioning.
12. Once all experimental conditions (pressure at 1,000 psi, flow rate at 1 L/ min, and temperature at 130 ^{o}F) are set, switch the flow line from injecting water to injecting 15% HCl acid and move the outline line to the spent acid container.
13. Inject 15% HCl acid for 10 minutes and record leak-off rate every minute at leak-off container, if any.
14. After acid injection is completed for 10 minutes, change fluid injection from 15% HCl acid to water to flush the system, turn-off the heater and monitor pH fluid at the outlet until its pH is neutral.
15. Once the pH fluid is neutral, remove the heating jacket, depressurize the system, and turn off the pump.
16. Dismantle all connections and side pistons, lift the acid injection cell and push out the core samples from the cell using the hydraulic jack with wooden block.
17. Clean up core samples (from water and acid) and put it into oven to make it dry. Clean up the cell from any residue of acid and sealant.
18. Scan with profilometer scanner for post injection condition.

Figure 14 Glass vessel with lid and vacuum equipment

Figure 15 Acid injection apparatus, hydraulic jack and its connections

2.5. Conductivity Measurement Experimental Procedures

In this study, after completing acid injection and surface scan profilometer, dolomite core samples were prepared for acid fracture conductivity measurement. Prior to conducting measurements, dolomite core samples were put together leaving some apertures created by acid etching, covered by silicone-based (detail procedure was explained in the 2.2 core sample preparation) and measured its acid fracture conductivity. The steps below explain the detailed procedure of acid fracture conductivity measurement:

1. Ensure that dolomite core samples, that have been prepared using detailed procedure in section 2.2, have 5 required-holes as inlet, outlet, and three different points of pressure transducers reading.
2. Wrap two layers of teflon tape around the core samples slightly below the top and above the bottom horizontally. Besides, wrap two layers of tape around the core samples vertically on two positions between each hole of three-hole for pressure transducer reading.
3. Apply silicone grease on the sides of the sample core.
4. Insert the sample core into conductivity cell using the hydraulic jack.
5. Insert two side pistons, which are top and bottom, into conductivity cell to prevent movement of the sample core when closure stress is applied by the load frame.
6. Place the conductivity cell in horizontal position in the center of the load frame to ensure even distribution of the force on the contact area as shown in the

Figure 16. Ensure that inlet, outlet and flow direction of nitrogen are the same with the one applied in acid injection experiment.

7. Lower the piston of the load frame until it touches the top piston of the cell. Set load frame to 1,000 psi.
8. Connect all the assembly and lines. Ensure that inlet valve is open and backpressure regulator is closed.
9. Open nitrogen tank and pressurize the cell to 30 psi. If there is a leak, fix and tighten the connection immediately.
10. Open back pressure regulator and set the first flow rate and record the cell pressure and differential pressure across fracture surface after stable condition.
11. Repeat step 10 for four times to obtain four different points of flow rate, pressure, and differential pressure at a certain closure pressure.
12. Increase closure stress to 8,000 by using step-changes for every 1,000 psi and repeat step 10 for each closure stress.
13. Turn off nitrogen flow and decrease closure stress to 1,000 psi.
14. At 1,000 psi, disassemble the conductivity cell and disconnect the lines.
15. Set closure stress to 0 psi and lift the load frame piston to remove two-side pistons and conductivity cell.
16. Push out the sample core using hydraulic jack and clean up the conductivity cell from grease and debris.

Figure 16 Acid fracture conductivity cell in the middle of loading frame of acid fracture conductivity measurement apparatus (Reprinted from Underwood 2013)

Based on data obtained from fracture conductivity measurement, acid fracture conductivity is calculated using the equation below.

$$\frac{(p_1^2-p_2^2)M}{2ZRTL} = \frac{1}{wk_f}\frac{\mu\rho q}{h} \quad (4)$$

This equation can be plotted as a straight line in a semi-log graph, $\frac{(p_1^2-p_2^2)M}{2ZRTL}$ vs $\frac{\mu\rho q}{h}$. The slope is the inverse of acid fracture conductivity and the difference of pressure squares is what is measured in the lab at four different flow rates (q) of each closure stress. Other constants used in the equation can be seen in the Appendix B.

3. RESULTS AND DISCUSSION

3.1. San Andres Dolomite Core Samples Characterization and Description

There were three measurements conducted to help analyze the results of acid fracture conductivity in this study. These three characterizations were XRD test, surface scan profilometer, and anhydrite's appearance on the fracture surface. These series of tests provided several parameters such as anhydrite content in core samples from XRD, acid-etched volume after acid injection from surface scan profilometer, and type of anhydrites of core samples used in the study from visual characterization of anhydrite presence on the fracture surface. These parameters were then correlated to acid fracture conductivity measured in the last step of experiments to evaluate how these parameters affected acid fracture conductivity.

In this study, XRD was carried out to identify mineralogy of dolomite sample cores. Each sample core was cut on the top of the fracture surfaces to make powder samples for XRD. Summary of the XRD results is shown in the Table 2.

Table 2 Summary of XRD result and anhydrite surface characterization

Test #	Surf Char	Etc Vol	Dolomite	Anhydrite	Quartz	Kaolinite	Chlorite	Illite	Oligoclase
Test-01	Bedded	0.222	74.33	18.87	1.98	4.82			
Test-02	Bedded	0.253	54.98	42.86	0.68	1.48			
Test-03	Patchy	0.217	55.8	43.04	0.57	0.59			
Test-04	Pore-filled	0.262	58.29	41.1	0.61	0			
Test-05	Pore-filled	0.379	67.28	30.75	0.75	1.22			
Test-06	Pore-filled	0.268	89.86	5.56	2.08	2.5			
Test-07	Patchy	0.236	69.67	28.8	0.82	0.71			
Test-08	Pore-filled	0.563	96.25	2.06	0.11				1.58
Test-09	Pore-filled	0.533	86	3.93	1.46		1.17	4.17	3.27
Test-10	Pore-filled	0.611	94.59	4.52	0.17				0.72
Test-11	Pore-filled	0.355	89.11	8.84	0.73				1.32
Test-12	Pore-filled	0.239	90.79	1.06	3.58			2.01	2.56

Based on XRD result, dolomite core samples used in the study comprised seven different minerals, which were dolomite, anhydrite, quartz, kaolinite, chlorite, illite, and oligoclase feldspar. These minerals had variations of percentage in dolomite core sample. In this study, anhydrite, which had variations from 1% to 43%, became the focus of investigation on how this mineral and its distribution affected acid fracture conductivity of dolomite core samples. Besides, referring to Crain's petrophysical handbook, Table 3 summarized the elastic properties of minerals which are present in the San Andres dolomite sample core.

Table 3 Elastic properties of minerals in the San Andres dolomite rocks

Rocks	Bulk Modulus	Shear Modulus	Young Modulus
	10^6 psi	10^6 psi	10^6 psi
Plagioclase	11.0	3.8	3.4
Calcite	11.2	4.6	4.1
Dolomite	13.8	6.5	5.6
Anhydrite	6.5	4.2	3.5
Clay	0.2	0.2	0.2
Quartz	5.4	6.5	4.6

In this study, anhydrite's patterns and distributions were characterized based on Lucia's classification of anhydrite distribution that have three types of distribution. Three types of distribution are as follows:

1. Patchy Distribution

   This anhydrite distribution consists of two type of anhydrite based on Lucia's classification, which are poikilotopic (A) and nodular (B) as shown in the Figure 17. Based on visual characterization of anhydrite distribution on fracture surfaces before acidizing and after conductivity, Test-3 and Test-7, as seen in the Figure 18 and 19, were categorized as patchy distribution. Large

nodules anhydrite could be clearly identified on the fracture surface at the initial condition or before acid injection. In addition to that, some parts of fracture surfaces turned out to be whitish after conductivity test indicating that other type of anhydrite, which may be poikilotopic, were present on the fracture surface.

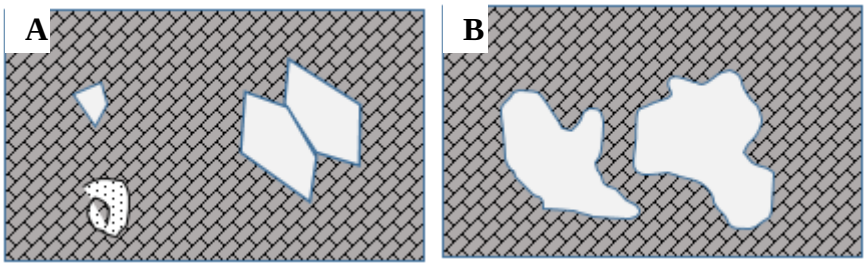

Figure 17 Patchy distribution consists of poikilotopic (a) and nodular (b) (Adapted from Lucia 1999)

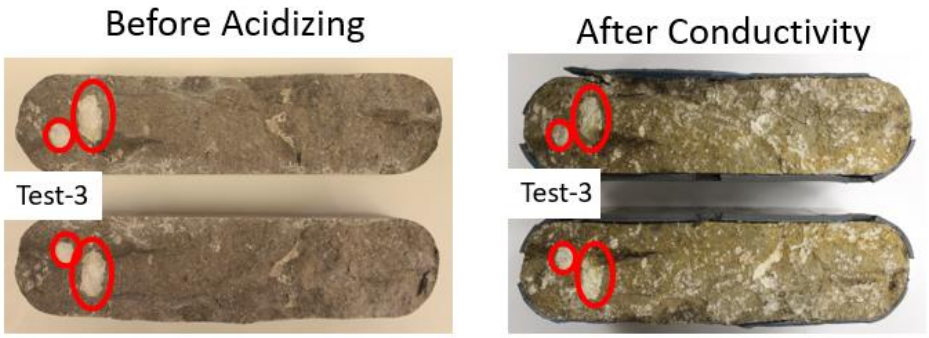

Figure 18 Surface characterization of Test-3 – patchy distribution

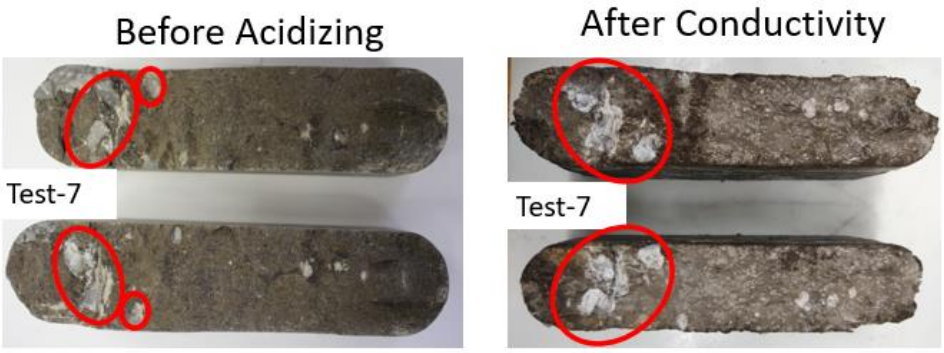

Figure 19 Surface characterization of Test-7 – patchy distribution

2. Pore-filled (even distribution)

   This anhydrite distribution typically was barely seen on the fracture surface at the initial condition because it was widely and finely distributed and filled throughout the pores as shown in the Figure 20. For some core samples, the anhydrite presence could only be obviously identified as some parts of fracture surfaces turned out to be whitish after conductivity test, as depicted in the Figure 21 to Figure 23, while other samples showed slightly whitish on the fracture surfaces as shown in the Figure 24 to Figure 28. This might be caused by the amount of anhydrite content varying from 1% to 41%. The core samples that turned out to be whitish had anhydrite content greater than 30% while other samples that were not clearly seen the anhydrite distribution had below 10% of anhydrite content. In this study, the majority of dolomite core samples were pore-filled type of anhydrite distribution.

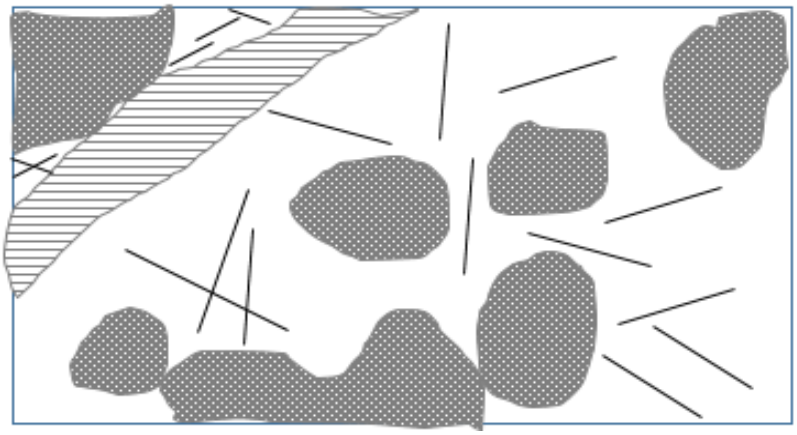

Figure 20 Pore-filled distribution (Adapted from Lucia 1999)

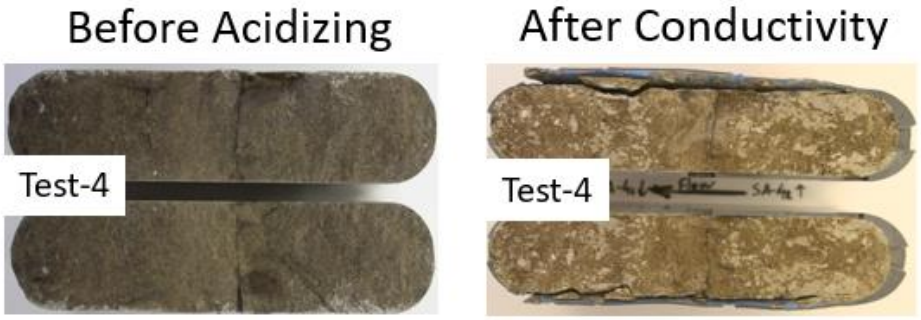

Figure 21 Surface characterization of test-4 – Pore-filled distribution

Figure 22 Surface characterization of test-5 – Pore-filled distribution

Figure 23 Surface characterization of test-6 – Pore-filled distribution

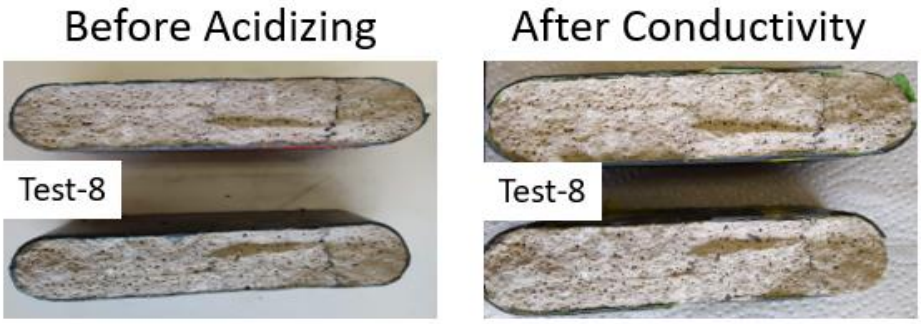

Figure 24 Surface characterization of test-8 – Pore-filled distribution

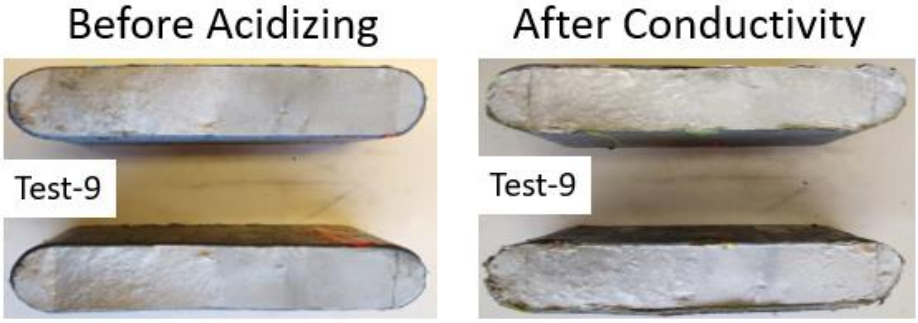

Figure 25 Surface characterization of test-9 – Pore-filled distribution

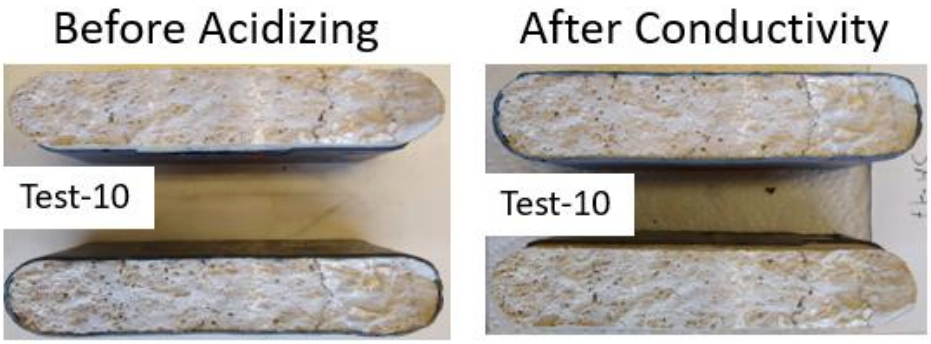

Figure 26 Surface characterization of test-10 – Pore-filled distribution

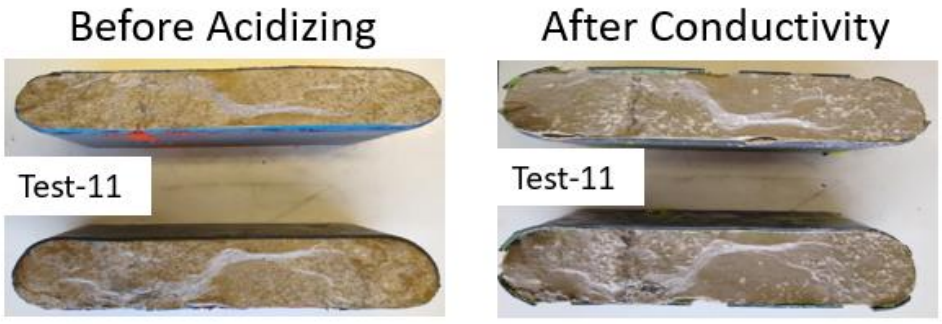

Figure 27 Surface characterization of test-11 – Pore-filled distribution

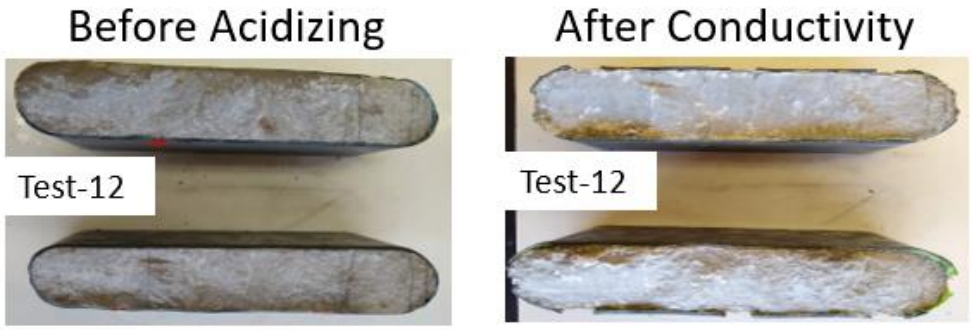

Figure 28 Surface characterization of test-12 – Pore-filled distribution

3. Bedded Anhydrite

This anhydrite distribution was found laterally continuous across the fracture surfaces which could be either laminated or composed of coalesced nodules as shown in the Figure 29. In this study, anhydrite distribution could be clearly identified as bedded anhydrite because it was clearly seen that anhydrite was diagonally and laterally distributed across the fracture surface and perpendicular to the flow direction as depicted in the Figure 30 and Figure 31. The perpendicular to the flow direction was caused by the vertical coring carried out to cut the downhole sample. This direction turned out to be parallel with the reservoir flow direction if this was position in the reservoir. Based on visual characterization, at the initial condition, some of the anhydrite distribution can be clearly identified and, after conductivity test, some parts of fracture surfaces revealed whitish surfaces distributed diagonally and laterally across the fracture surfaces.

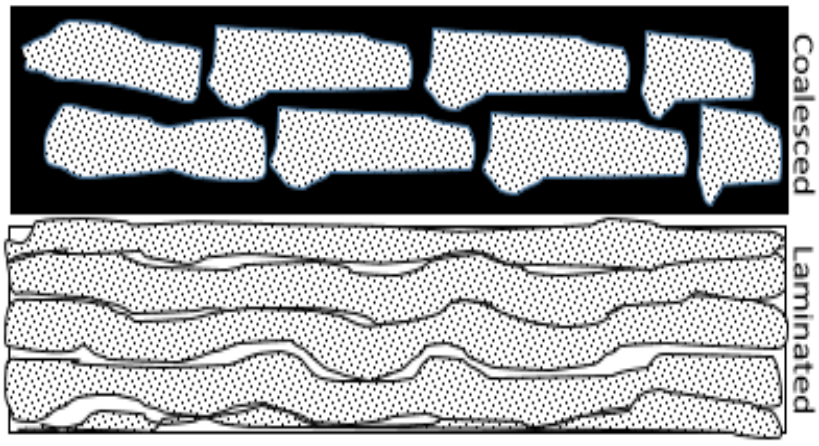

Figure 29 Bedded anhydrite distribution (Adapted from Lucia 1999)

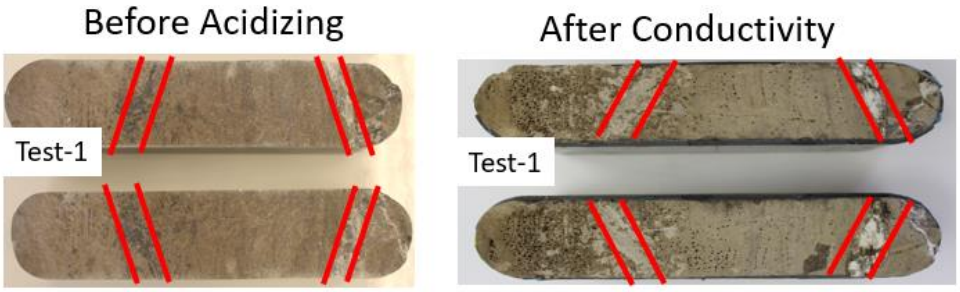

Figure 30 Surface characterization of test-1 – bedded anhydrite distribution perpendicular to the flow

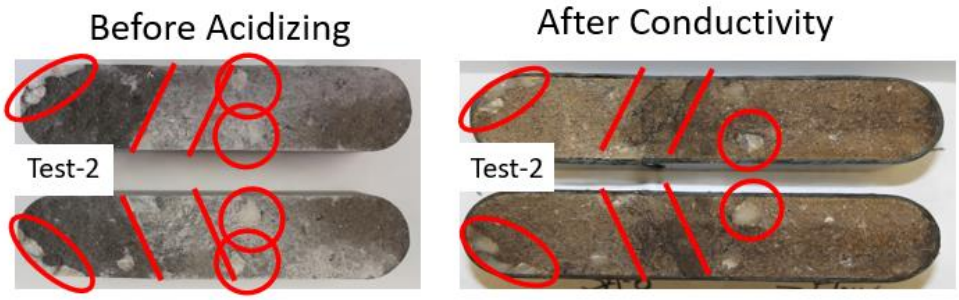

Figure 31 Surface characterization of test-2 – bedded anhydrite distribution perpendicular to the flow

3.2. Acid Etched Volume and Acid Fracture Conductivity Results and Comparisons

In this study, surface scan profilometer was carried out before and after acid injection to measure and compare the topography of fracture surfaces in order to calculate acid etched-volume based on the difference of it. Dolomite core samples were etched by 15% HCL regular acid with temperature 130 ºF, pressure 1,000 psi, injection time 10 minutes, and flow rate 1 L/ min. These operating parameters were applied to all dolomite core samples. The result of surface scan profilometer is shown in the Figure 32 as an example. The remaining results of surface scan profilometer can be seen in the Appendix A.

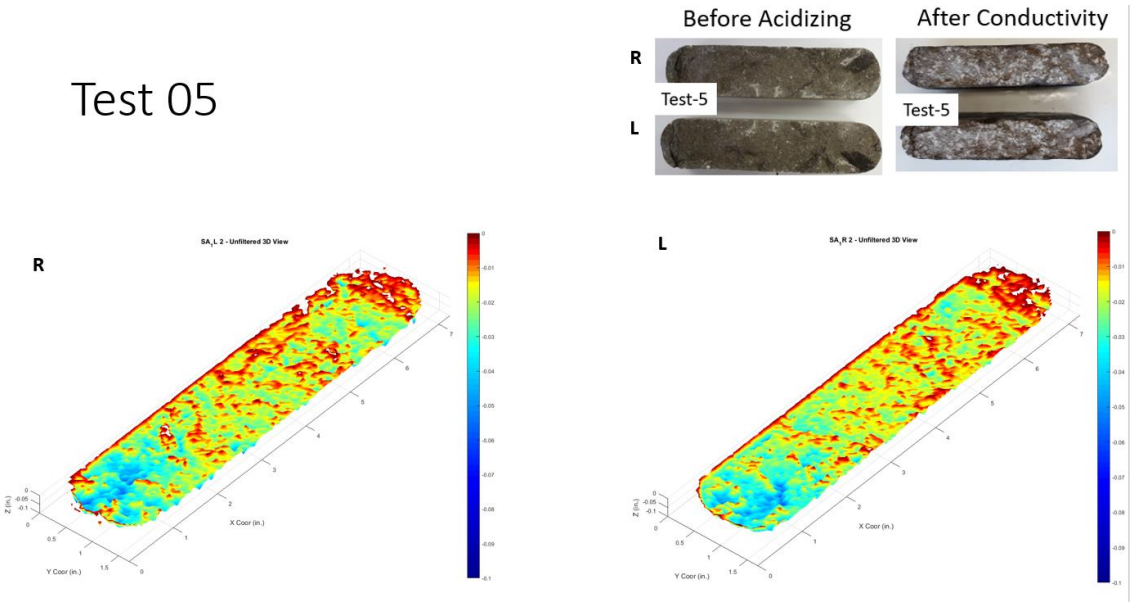

Figure 32 Acid etched profile of test-05

Based on surface scan profilometer results, acid etched pattern of each sample is unique and different from one to the others because they have their own mineralogy distribution on the fracture surfaces and there are no surface scan profilometer that have exactly the same acid etched pattern. Besides, the value of acid etched volume is also unique and different for every pair of dolomite core samples. These acid etched volume results were summarized in the following Table 4.

Table 4 Summary of acid etched volume

Test #	Surf Char	Etc Vol	Dolomite	Anhydrite	Non Anhydrite
Test-01	Bedded	0.222	74.33	18.87	6.8
Test-02	Bedded	0.253	54.98	42.86	2.16
Test-03	Patchy	0.217	55.8	43.04	1.16
Test-04	Pore-filled	0.262	58.29	41.1	0.61
Test-05	Pore-filled	0.379	67.28	30.75	1.97
Test-06	Pore-filled	0.268	89.86	5.56	4.58
Test-07	Patchy	0.236	69.67	28.8	1.53
Test-08	Pore-filled	0.563	96.25	2.06	1.69
Test-09	Pore-filled	0.533	86	3.93	10.07
Test-10	Pore-filled	0.611	94.59	4.52	0.89
Test-11	Pore-filled	0.355	89.11	8.84	2.05
Test-12	Pore-filled	0.239	90.79	1.06	8.15

Based on acid etched volume and XRD results, both results were plotted together to see how good the correlations between acid etched volume to the content of mineralogy, both dolomite and anhydrite. Figure 33 and Figure 34 showed that there were no good correlations between acid etched volume and mineralogy indicated by R^2 of both correlations were low. This is probably caused by the mineralogy constitutes dolomite sample cores that it is not only dolomite and anhydrite but also there are other non-anhydrite minerals on the fracture surfaces, such as clay (kaolinite, chlorite, and illite), quartz, and oligoclase feldspar, that may influence the amount of volume of minerals soluble in the 15% HCl regular acid. However, if non-anhydrite minerals, which had greater than 2% content, were removed, the correlation of acid etched volume over anhydrite and dolomite showed better correlation as shown in the Figure 35 and Figure 36 and indicated by the increase of R^2 from 0.4 to 0.8.

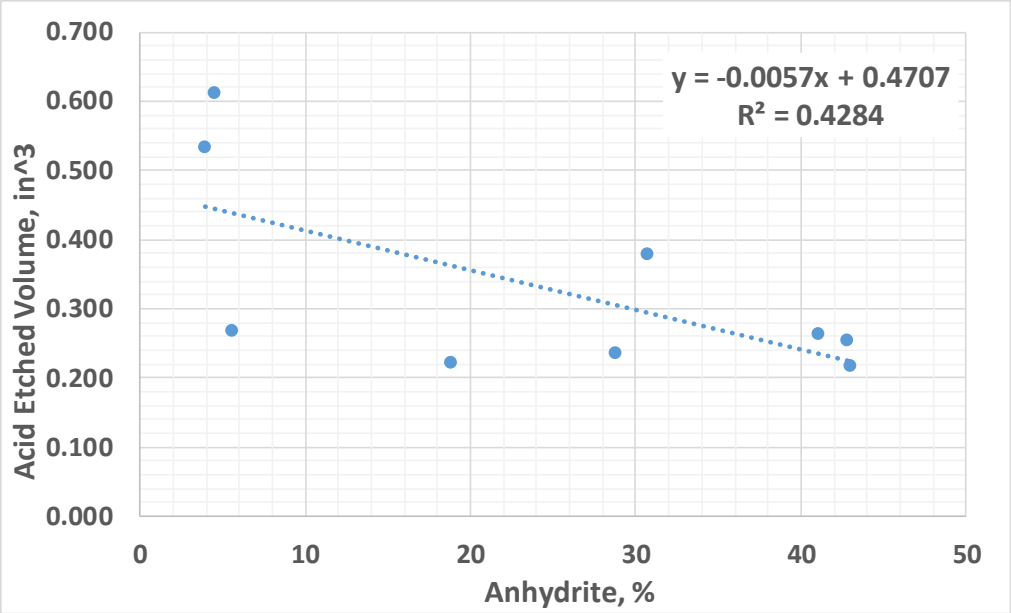

Figure 33 Correlation between anhydrite and acid etched volume

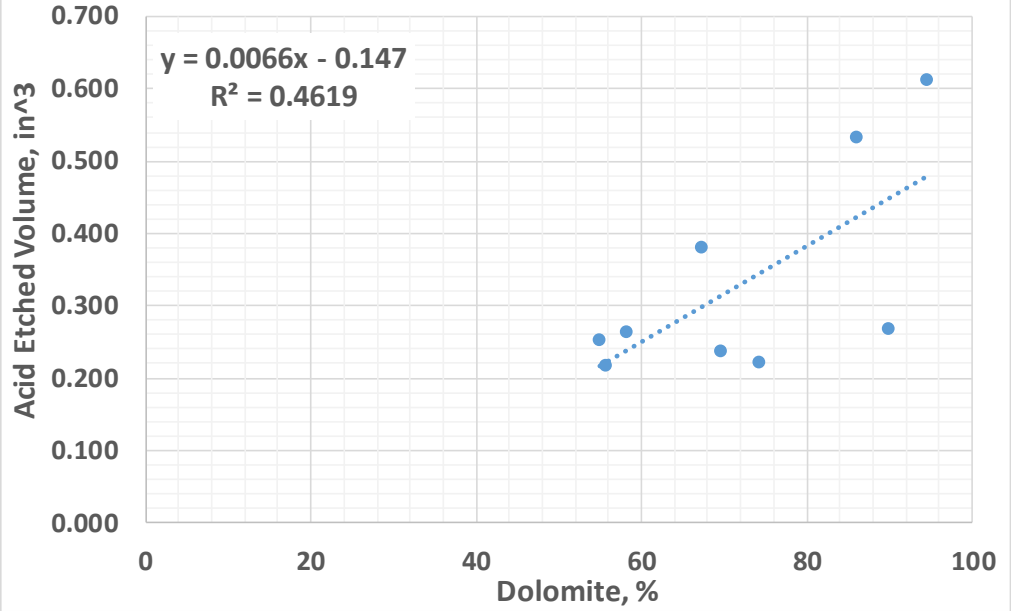

Figure 34 Correlation between dolomite and acid etched volume

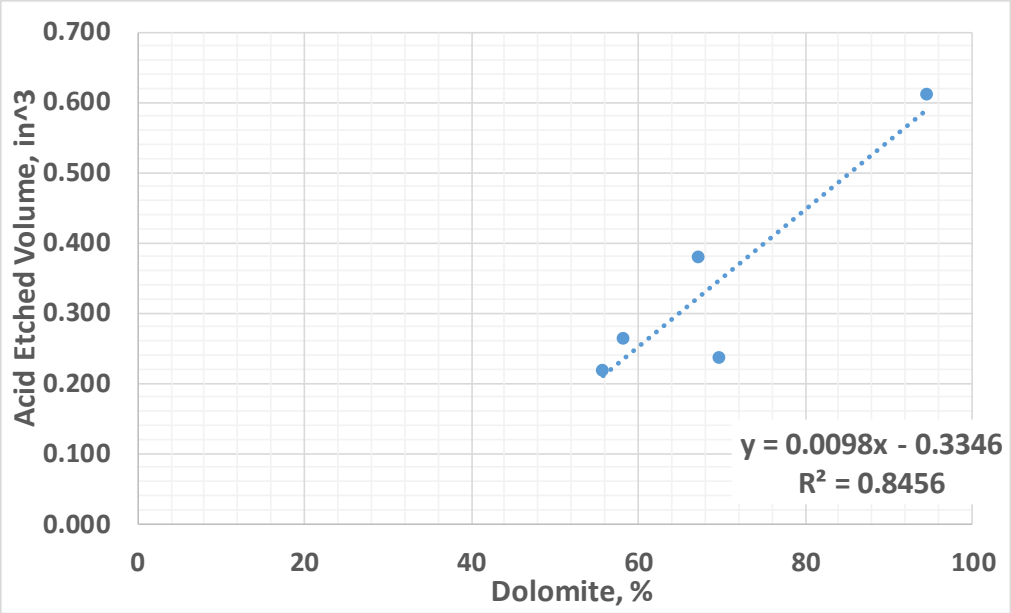

Figure 35 Correlation between dolomite and acid etched volume after removing non-anhydrite content greater than 2%

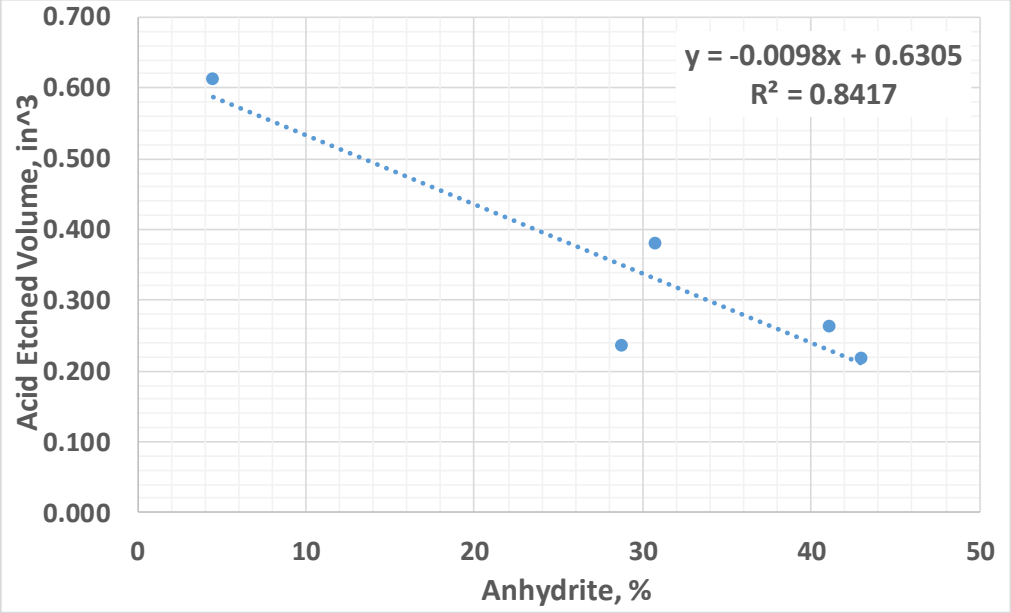

Figure 36 Correlation between anhydrite and acid etched volume after removing non-anhydrite content greater than 2%

After injecting acid and measuring the topography of the fracture surfaces before and after acid injection, the final parameter of this study, which was acid fracture conductivity, was measured for all dolomite core samples. The acid fracture conductivity was measured over several different closure stresses, which were 1,000 psi to 8,000 psi. However, only 6 core samples completed for that closure stresses range. The remaining dolomite core samples were completed with different closure stresses range, which were as follows:

1. The first three core samples completed with closure stresses ranged from 1,000 psi to 3,000 psi before extending closure stresses to 8,000 psi.
2. There were three core samples that broke at certain closure stress and was unable to continue the experiment with breaking dolomite core samples condition that would lead to continuously increase acid fracture conductivity as closure stresses increase. One core sample broke at 1,500 psi closure stress and the remaining core samples broke at 5,000 – 6,000 psi closure stresses.

To further study the effect of anhydrite distribution on dolomite core samples, acid fracture conductivity decline rate, acid fracture conductivity at zero closure stress, and selected closure stress that represented field closure stress were discussed and evaluated based on anhydrite distribution on the fracture surfaces to evaluate the impact of anhydrite distribution on acid fracture conductivity of dolomite core samples that had anhydrite distribution on its fracture surfaces. Closure stress at 3,000 psi was selected for point of evaluation since at this point was believed as the actual closure stress value of San Andres

dolomite formation that was commonly used in the application of acid fracture design in this formation.

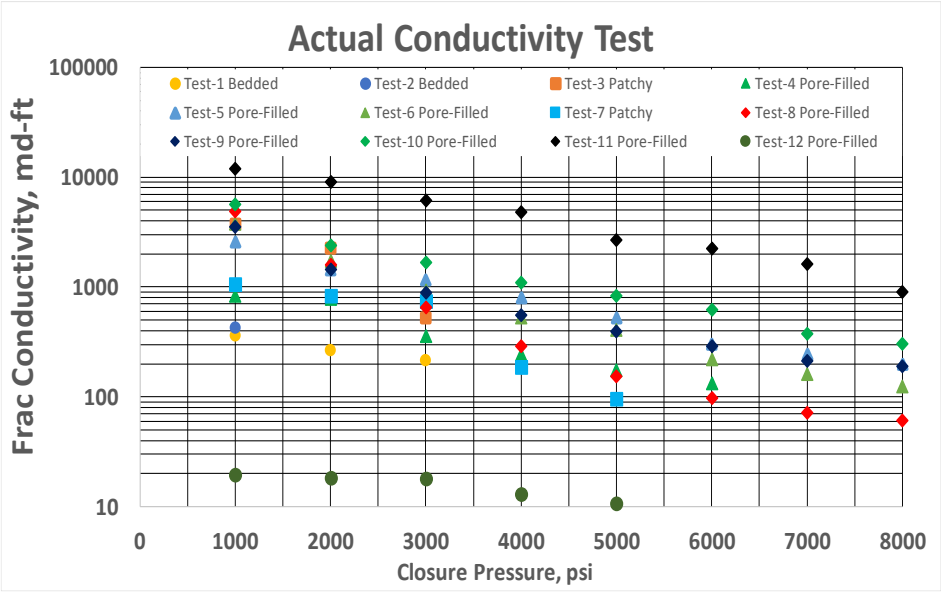

Figure 37 All acid fracture conductivity for all San Andres dolomite core samples

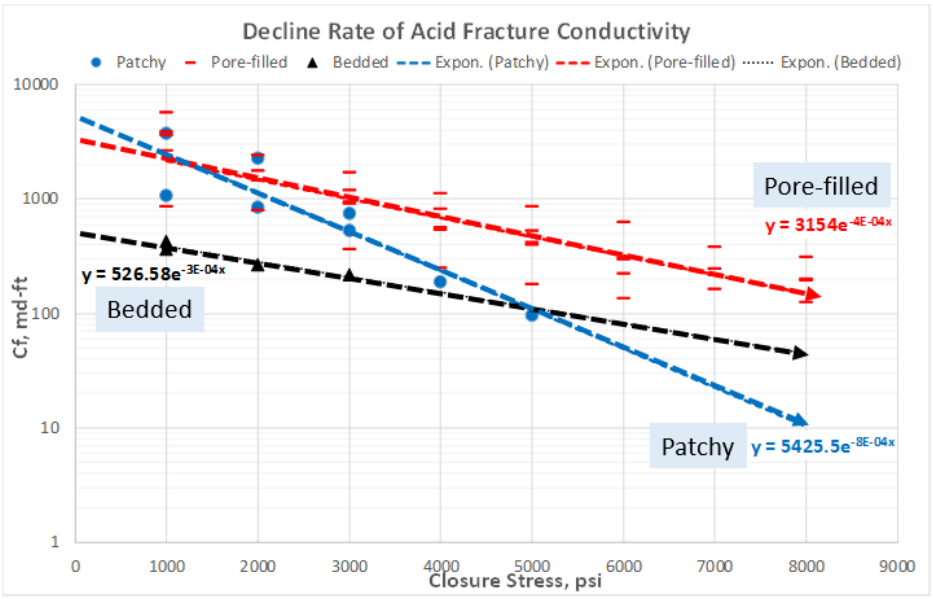

Figure 38 Decline rate of acid fracture conductivity based on anhydrite distribution

Figure 37 showed acid fracture conductivity test for all San Andres dolomite core samples and Figure 38 showed acid fracture conductivity decline of San Andres dolomite core samples could be categorized into three different type corresponding to anhydrite distribution on the fracture surfaces, which were patchy distribution, pore-filled distribution, and bedded-anhydrite distribution that perpendicular to the fluid flow. Besides, Figure 37 showed that there were two San Andres dolomite core samples which were considered as an outlier and excluded in the analysis because both acid fracture conductivity results were too low (test-12) and too high (test-11). In addition to that, there was one sample (test-8) considered as outlier and excluded from the analysis because it had leaking problem while injecting acid. Therefore, only 9 San Andres dolomite core samples were plotted into the three different chart corresponding to the anhydrite distribution.

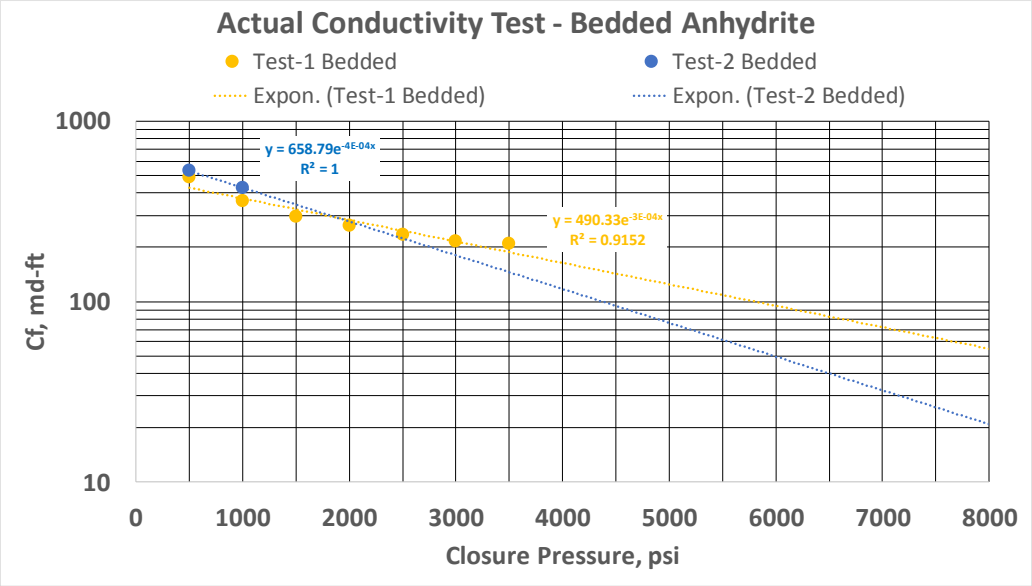

Figure 39 Acid fracture conductivity for bedded anhydrite distribution

Figure 39 showed acid fracture conductivity for bedded-anhydrite distribution that is perpendicular to the fluid flow. There were two core samples categorized into this distribution group, which are test-1 and test-2. One core sample, test-2, could only withstand until 1,000 psi closure stress because it broke at 1,500 psi and resulted in higher acid fracture conductivity than previous closure stress that would lead to erroneous conclusion since it was the opposite of acid fracture conductivity results from many past experiments that it was declined exponentially. Another core sample, test-1, could last until end of experiment but this experiment was carried out in the beginning of this study and it still used 3,500 psi as a final closure stress applied in the experiment. This anhydrite distribution had the lowest acid fracture conductivity at zero closure stress (400 – 650 md-ft) and 3,000 psi (216 md-ft), but it had the lowest decline rate of acid fracture conductivity ($3 \times 10^{-4}\ psi^{-1}$). The lowest value of acid fracture conductivity at this anhydrite distribution was probably caused by the presence of anhydrite that was perpendicular to the fluid flow caused additional restriction for fluid to flow. This perpendicular position came from the sample core which was carried out coring process in the vertical well, then the slab core was cut based on required-dimension for the experiment as explained in chapter 2. Hence the presence of bedded anhydrite was perpendicular to the fluid flow. However, if this was viewed from reservoir point of view, the presence of bedded anhydrite would be parallel to the fluid flow and not prevent fluid to flow that provide conductivity as illustrated in the Figure 40, so acid fracture conductivity of bedded anhydrite might be higher in the reservoir (parallel to the flow) than in the laboratory (perpendicular to the flow).

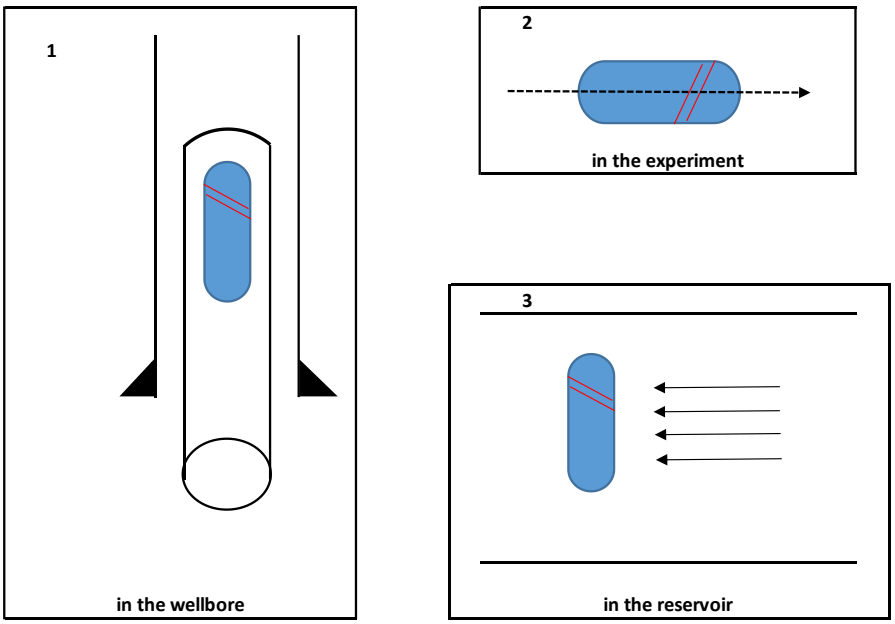

Figure 40 Different view of bedded anhydrite from the wellbore during coring and in the experiment and in the reservoir including its flow direction marked by arrow

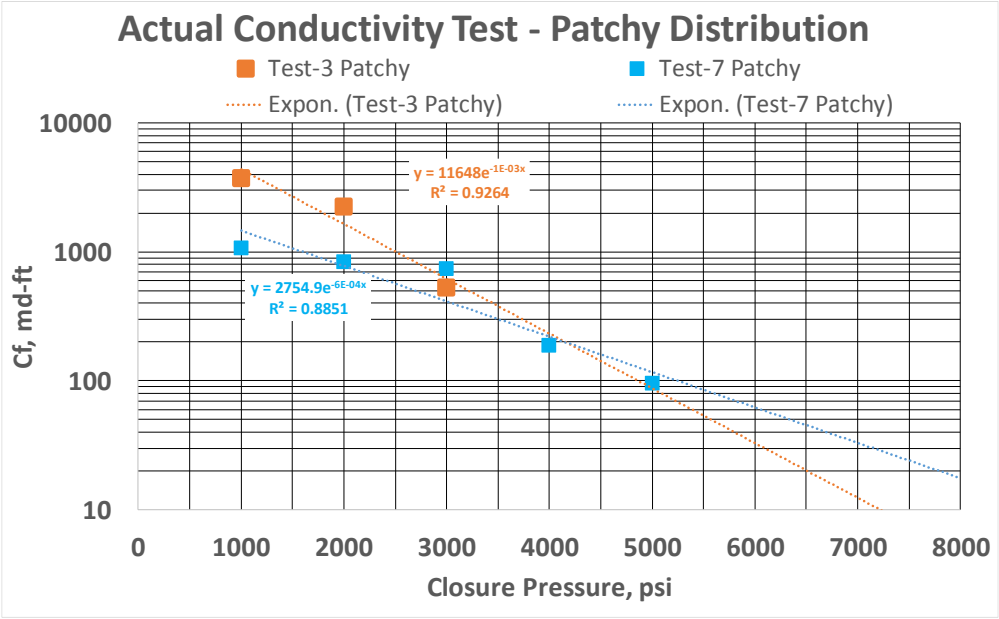

Figure 41 Acid fracture conductivity for patchy distribution

Figure 41 shows acid fracture conductivity for patchy distribution. There were two core samples categorized in this distribution group, which were test-3 and test-7. One core sample, test-3, was run until 3,000 psi closure stress because it was the first of three samples run only to 3,000 psi. Another sample, test-7, could only last until 5,000 psi and the sample broke because acid fracture conductivity started to increase and go higher than previous closure stress. This anhydrite distribution had higher and wider range of acid fracture conductivity at zero closure stress, which were from 2,500 md-ft to 12,000 md-ft. Besides, it had higher acid fracture conductivity decline rate, which were from 6×10^{-4} psi to $10 \times 10^{-4}\ psi^{-1}$, and higher value of acid fracture conductivity at 3,000 psi, which were from 350 md-ft to 750 md-ft.

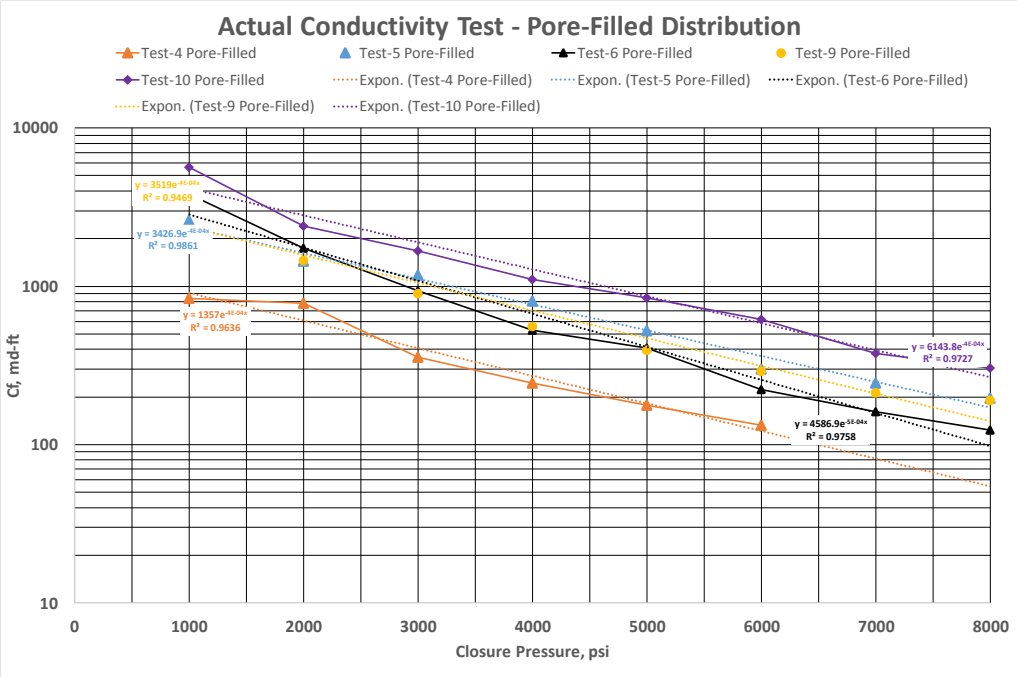

Figure 42 Acid fracture conductivity for pore-filled distribution

Figure 42 showed acid fracture conductivity for pore-filled distribution. There were eight core samples categorized in this distribution group, which were test-3 to test-6 and test-8 to test-12. However, there were three samples (test-8, test-11, and test-12) excluded in the analysis because these three samples were considered as an outlier and had a problem in the experimental works that would mislead the evaluation's result. Most of the pore-filled samples could run the experiment until 8,000 psi and only one sample that was run until 6,000 psi. This anhydrite distribution had lower and narrower range of acid fracture conductivity at zero closure stress, which were from 1,350 md-ft to 6,150 md-ft, than patchy distribution but higher than bedded anhydrite. Besides, it also had lower acid fracture conductivity decline rate than patchy distribution but higher than bedded anhydrite, which were from $4 \times 10^{-4}\ psi^{-1}$ to $5 \times 10^{-4}\ psi^{-1}$, and highest and widest value of acid fracture conductivity at 3,000 psi, which were from 350 md-ft to 1,650 md-ft. All of these acid fracture conductivity data were compared in the same plot as depicted in the Table 5 and Figure 43.

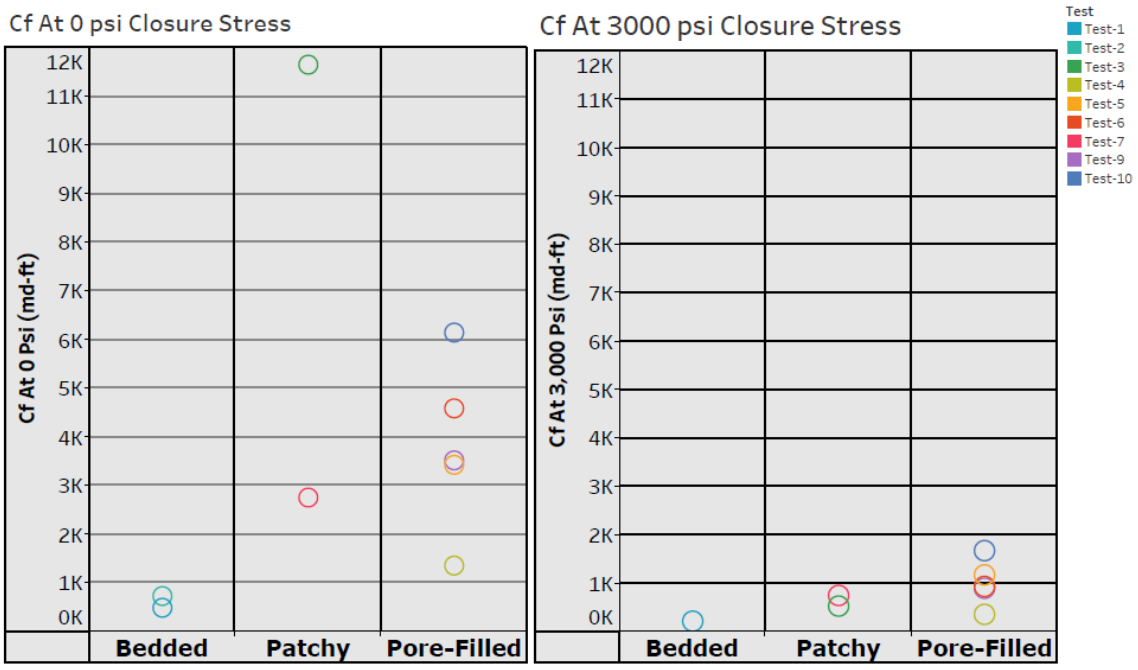

Figure 43 Comparison of acid fracture conductivity at 0 psi and 3,000 psi for all types of anhydrite distribution

Table 5 Summary of acid fracture conductivity at 0 psi, at 3,000 psi, and its slope value

Test	at 3,000 psi	Etched Vol	%Dolomite	% Anhydrite	Distribution	at 0 psi	Slope
Test-1	216.0	0.222	74.33	18.87	Bedded	490.3	3.00E-04
Test-2	0.0	0.253	54.98	42.86	Bedded	731.2	6.00E-04
Test-3	528.0	0.217	55.8	43.04	Patchy	11,648.0	1.00E-03
Test-4	357.0	0.262	58.29	41.1	Pore-Filled	1,357.0	4.00E-04
Test-5	1,173.0	0.379	67.28	30.75	Pore-Filled	3,426.9	4.00E-04
Test-6	934.0	0.268	89.86	5.56	Pore-Filled	4,586.9	5.00E-04
Test-7	748.0	0.236	69.67	28.8	Patchy	2,754.9	6.00E-04
Test-9	897.5	0.533	86	3.93	Pore-Filled	3,519.0	4.00E-04
Test-10	1,674.0	0.611	94.59	4.52	Pore-Filled	6,143.8	4.00E-04

Based on Table 5, acid fracture conductivity at 3,000 psi and 0 psi were plotted with several parameters such as acid etched volume, % dolomite and % anhydrite in order to see how these parameters affect acid fracture conductivity. Figure 44 to Figure 46

showed three plots of acid fracture conductivity at 3,000 psi over acid etched volume, percentage of dolomite, and percentage of anhydrite, respectively. These plots showed that there were poor correlations between acid fracture conductivity and plotted-parameters as R^2 showed lower value indicating weak correlations. Besides, Figure 47 to Figure 49 showed three plots of acid fracture conductivity at 0 psi over acid etched volume, percentage of dolomite and percentage of anhydrite, respectively. These plots have the same result as acid fracture conductivity at 3,000 psi that there were poor correlations between acid fracture conductivity at 0 psi and plotted-parameters.

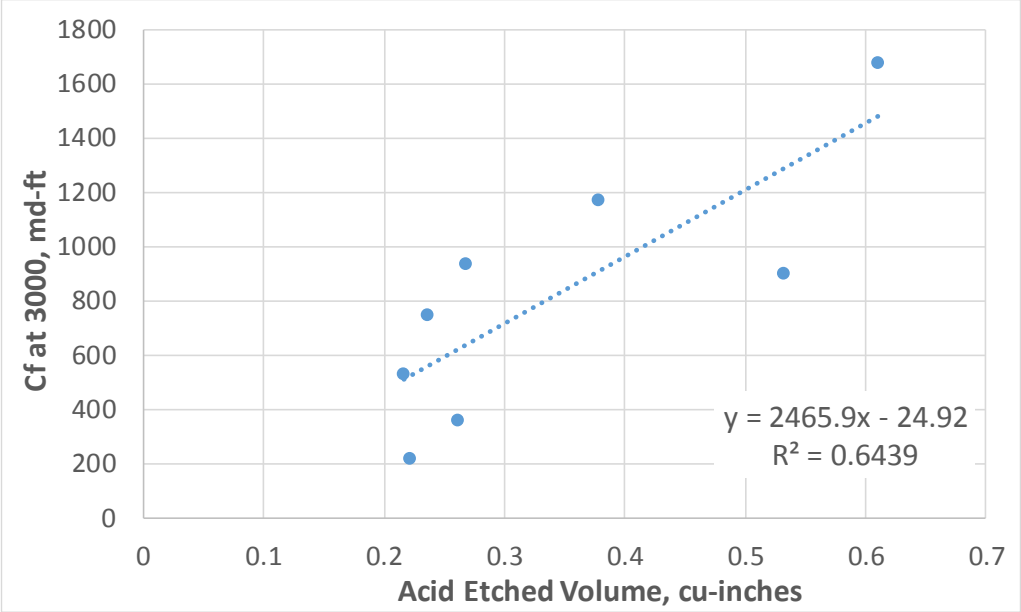

Figure 44 Fracture conductivity variance at 3,000 psi with acid etched volume

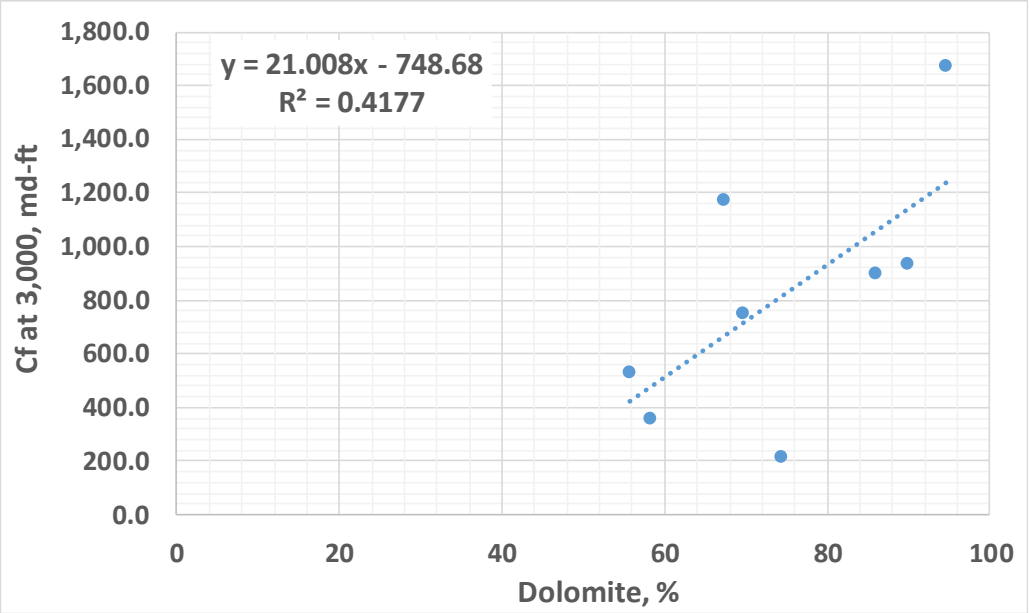

Figure 45 Fracture conductivity at 3,000 psi as a function of dolomite %

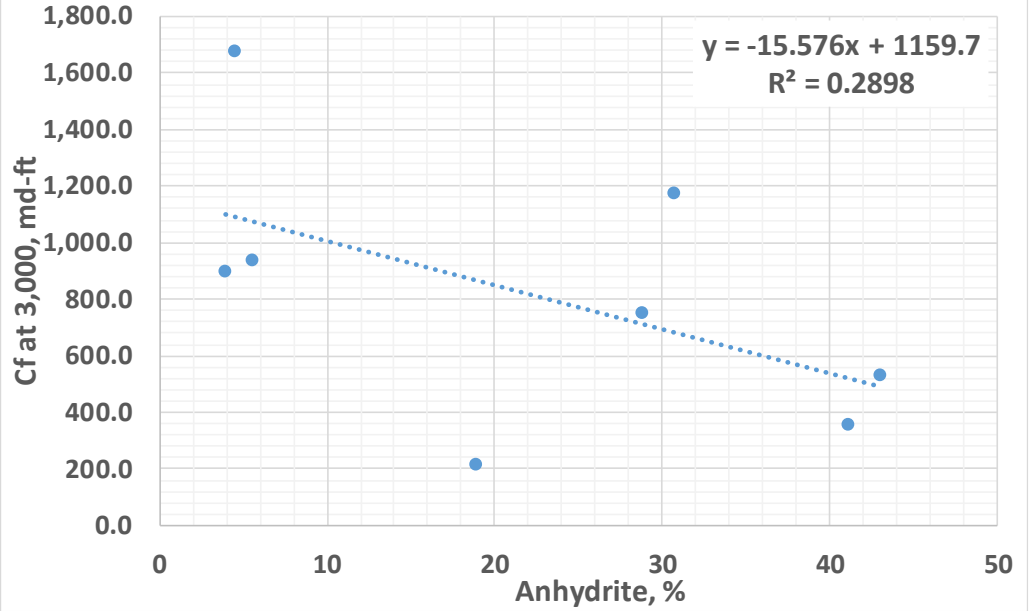

Figure 46 Fracture conductivity at 3,000 psi as a function of anhydrite %

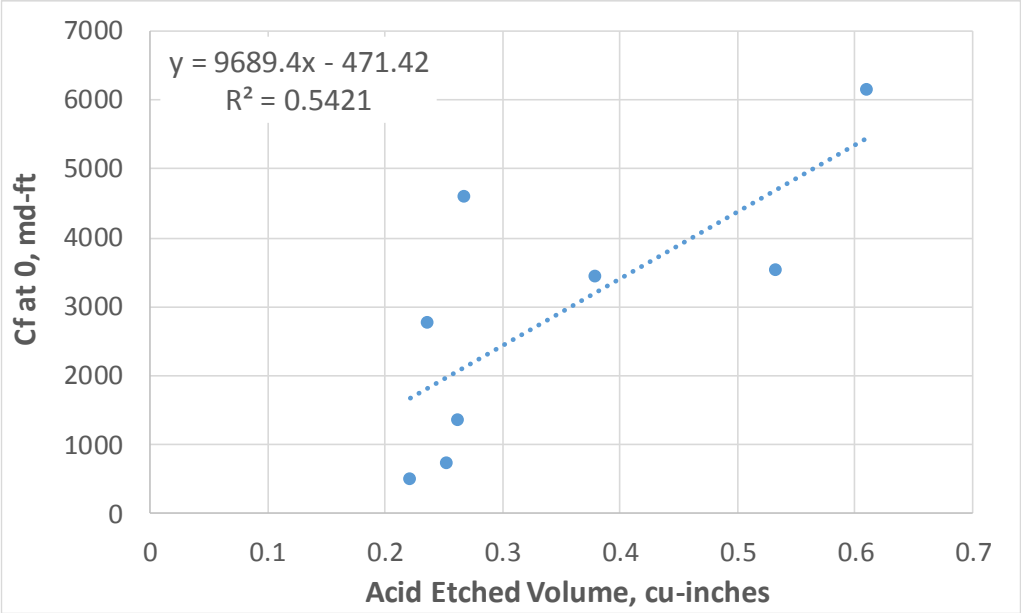

Figure 47 Fracture conductivity variance at 0 psi with acid etched volume

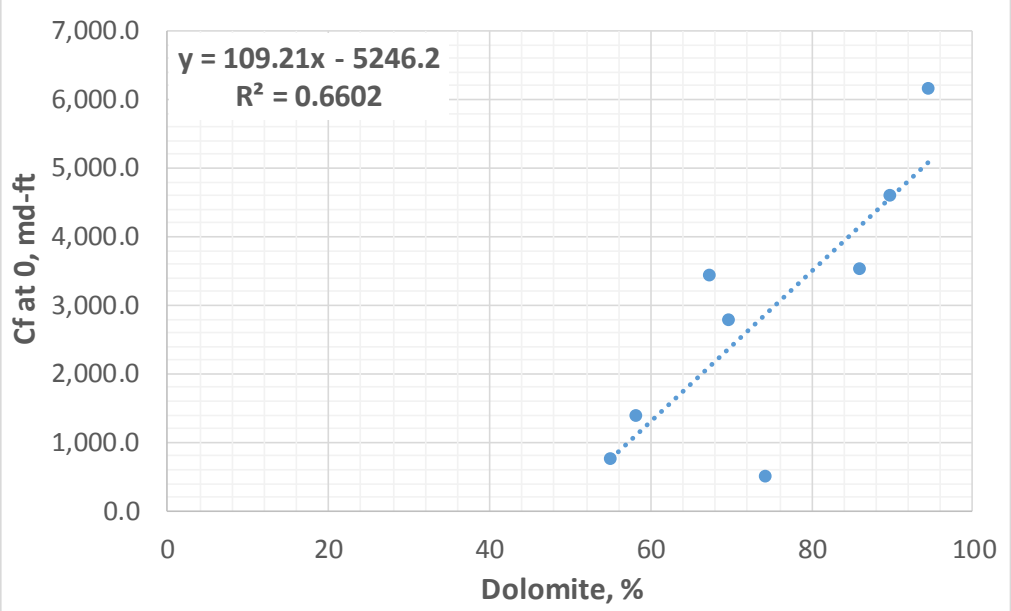

Figure 48 Acid fracture conductivity at 0 psi as a function of dolomite %

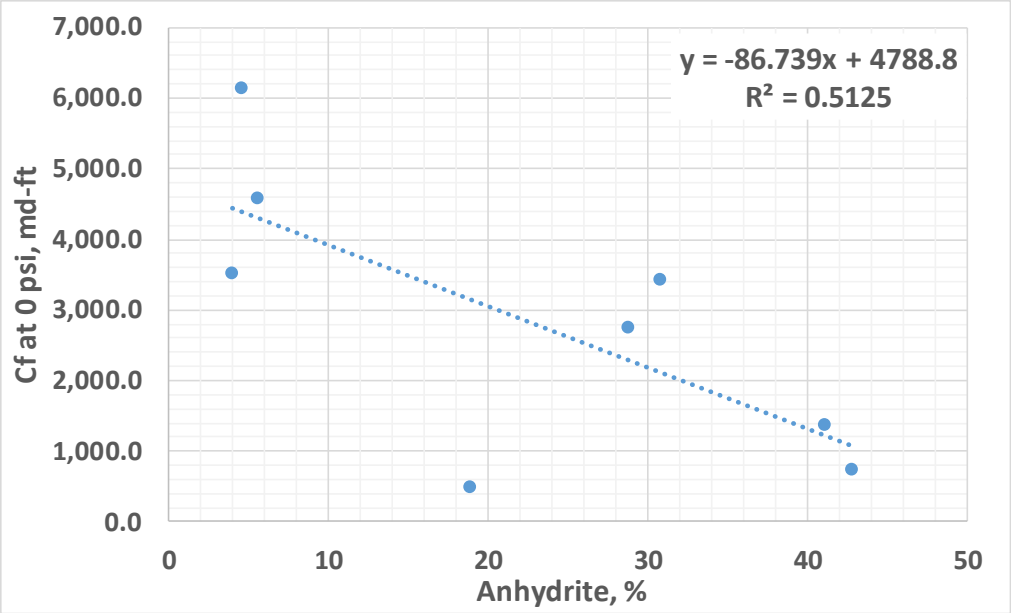

Figure 49 Acid fracture conductivity at 0 psi as a function of anhydrite %

Applying the same method as analyzing the correlation between acid etched volume and mineralogy, samples with non-anhydrite greater than 2% and outlier value greater than upper quartile adds interquartile range were removed to clean the data in order to evaluate the correlation of acid fracture conductivity over acid etched volume and percentage of mineralogy. After that, Figure 50 to Figure 52 showed the improvement of R^2 for acid fracture conductivity at 3,000 psi over acid etched volume, percentage of dolomite, and percentage of anhydrite, respectively. This was indicating that there were good correlations between acid fracture conductivity and plotted-parameters. This was applied to acid fracture conductivity at 0 psi as seen in Figure 53 to Figure 55. Based on the new plotted-data of acid fracture conductivity at 0 psi and 3,000 psi over acid etched volume, percentage of dolomite and percentage of anhydrite, acid fracture conductivity is proportional to the acid etched volume and the percentage of dolomite as the higher acid

etched volume and percentage of dolomite, the higher acid fracture conductivity. However, acid fracture conductivity is inversely proportional to the percentage of anhydrite as the higher percentage of anhydrite, the smaller acid fracture conductivity. These correlations are probably caused by the difference of elastic properties between anhydrite and dolomite. As seen in Table 3, young modulus of anhydrite is lower than dolomite which means that anhydrite cannot help sustaining the aperture of fracture that provides the conductive path for fluid flow. Consequently, the increasing percentage of anhydrite in dolomite rocks will decrease the acid fracture conductivity.

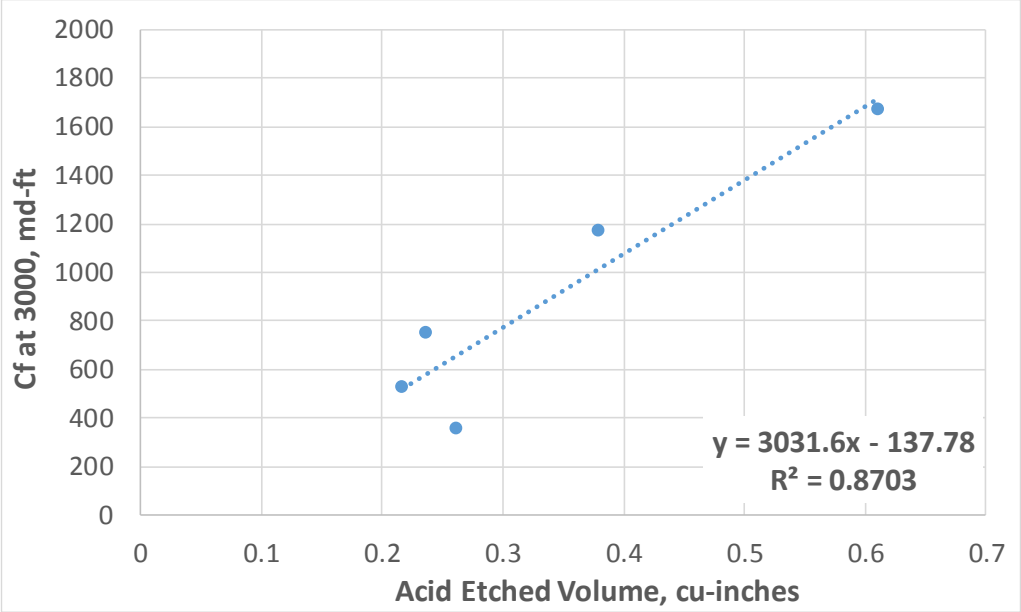

Figure 50 Fracture conductivity variance at 3,000 psi with acid etched volume after data cleansing

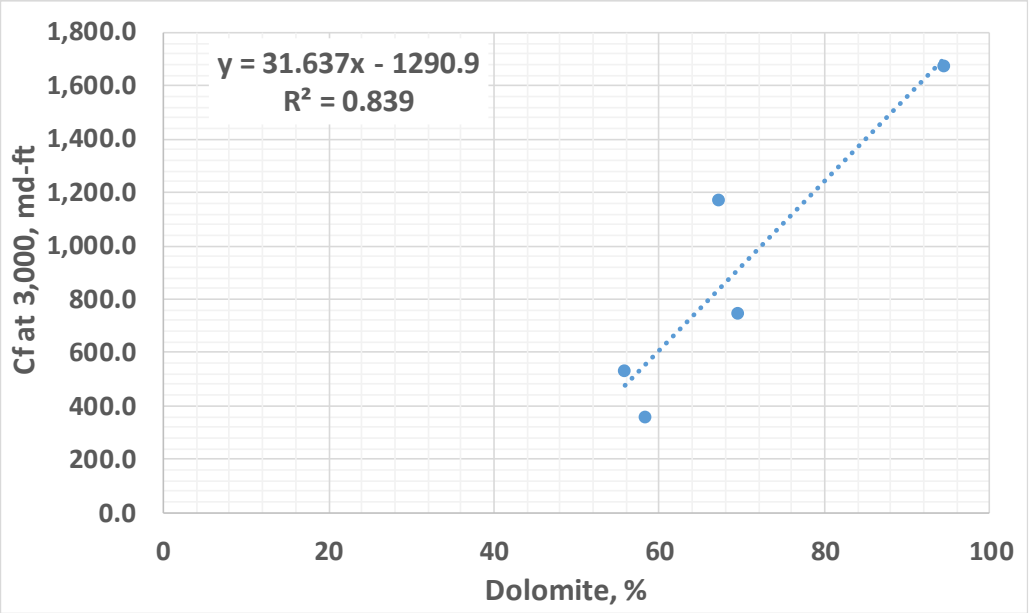

Figure 51 Acid fracture conductivity at 3,000 psi as a function of dolomite % after data cleansing

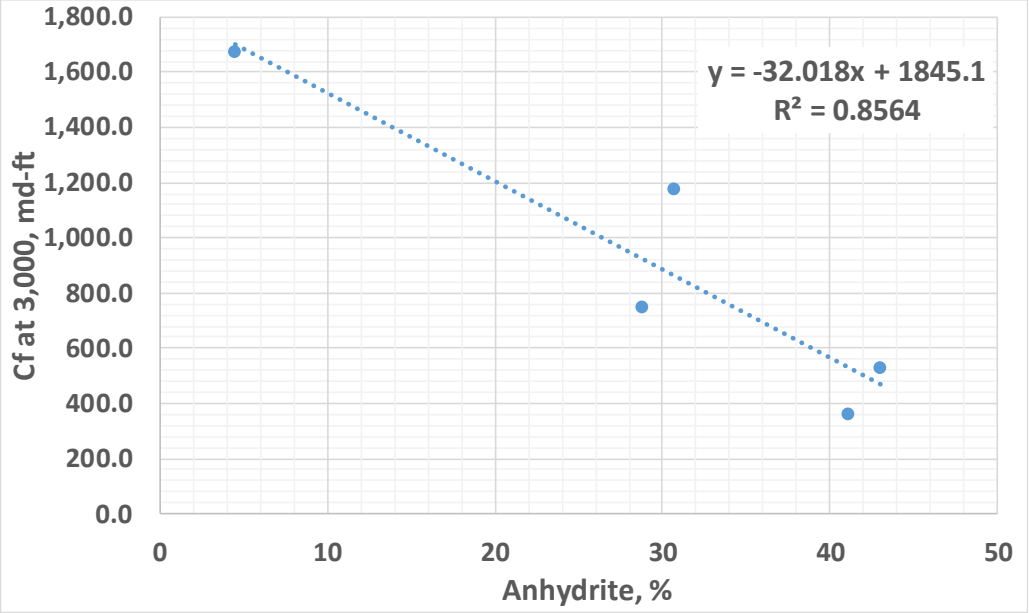

Figure 52 Acid fracture conductivity at 3,000 psi as a function of anhydrite % after data cleansing

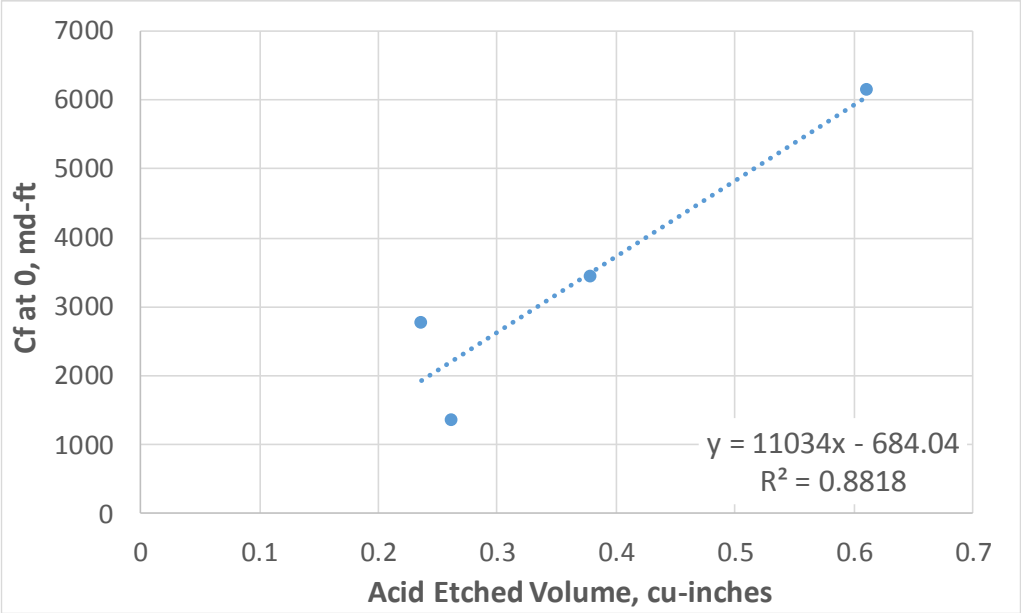

Figure 53 Fracture conductivity variance at 0 psi with acid etched volume after data cleansing

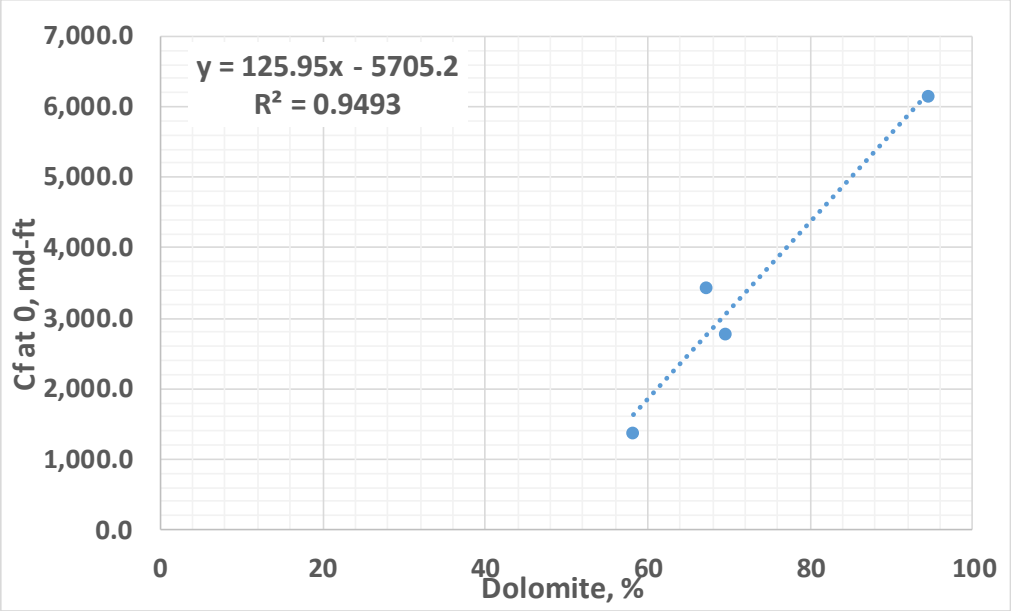

Figure 54 Acid fracture conductivity at 0 psi as a function of dolomite % after data cleansing

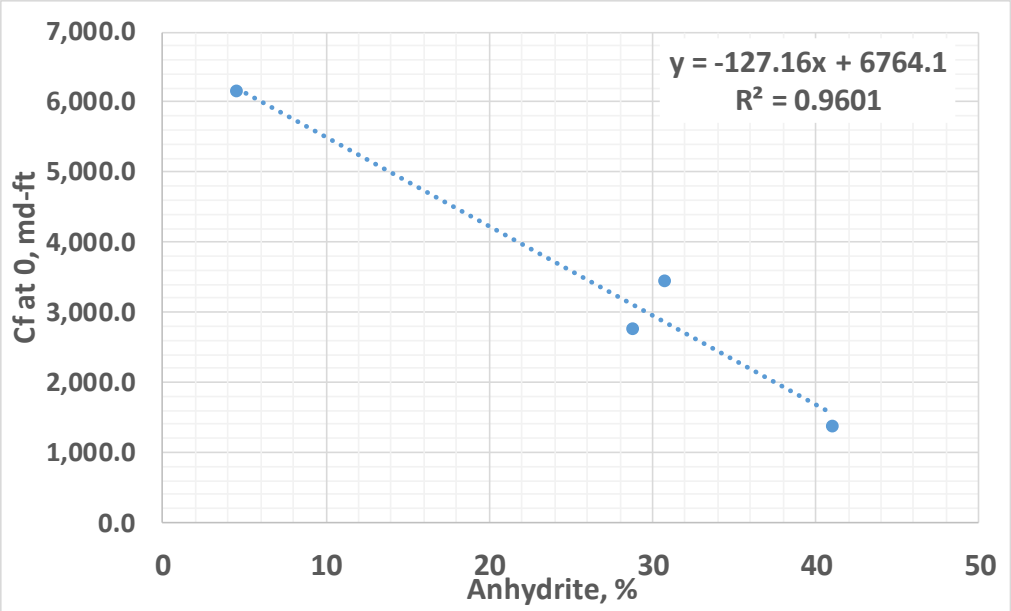

Figure 55 Acid fracture conductivity at 0 psi as a function of anhydrite % after data cleansing

3.3. Acid Fracture Conductivity Comparison with Other Rock Types

After comparing acid fracture conductivity for each anhydrite distribution, other comparisons were carried out by comparing acid fracture conductivity of anhydrite distribution with other rock types such as chalk, limestone, and outcrop dolomite and its acid fracture conductivity at 3,000 psi closure stress from past experiments such as Suleimenova (2015), Jin (2019), Melendez (2007), Penaloza (2013), Underwood (2013), and Wang (2015). Figure 56 and Figure 59 showed these comparisons for all acid fracture conductivity and acid fracture conductivity at 3,000 psi closure, respectively. Based on these comparisons, San Andres dolomite with anhydrite distribution on the fracture surface is good candidate for acid fracturing because it has good acid fracture conductivity value compared with limestone and outcrop dolomite.

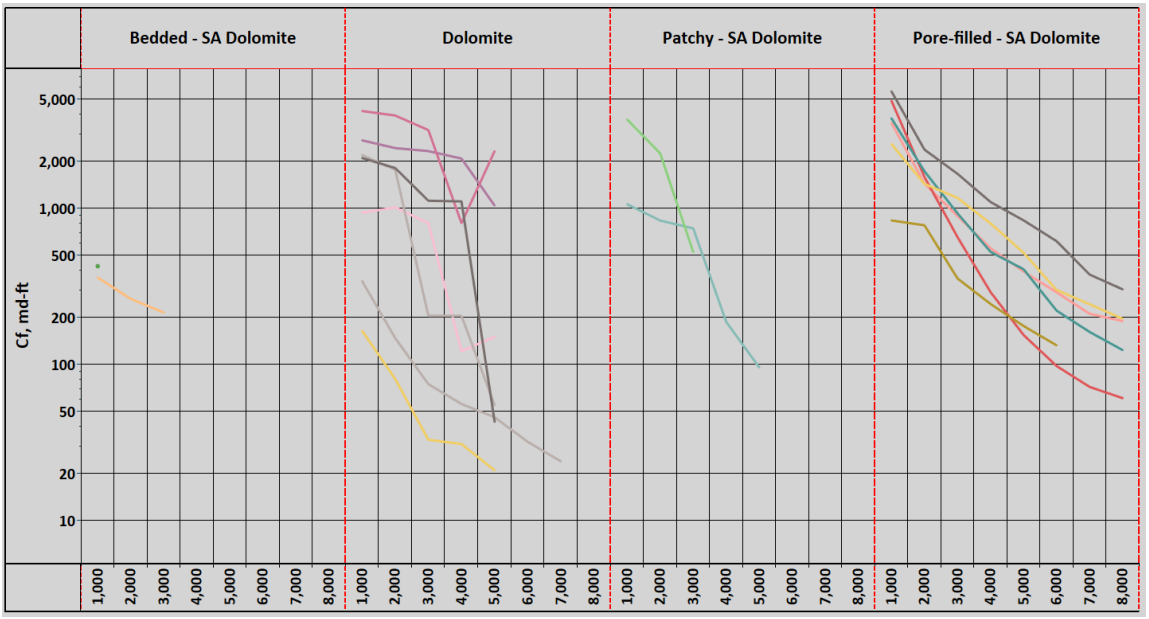

Figure 56 San Andres dolomite acid fracture conductivity comparison with San Andres dolomite outcrop

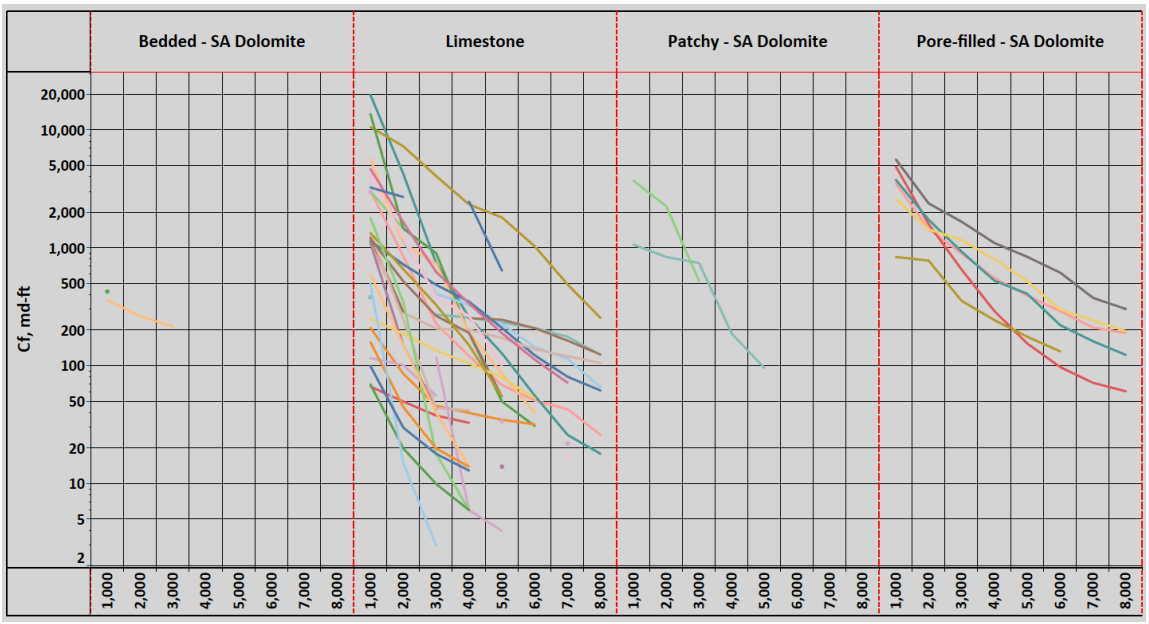

Figure 57 San Andres dolomite acid fracture conductivity comparison with limestone

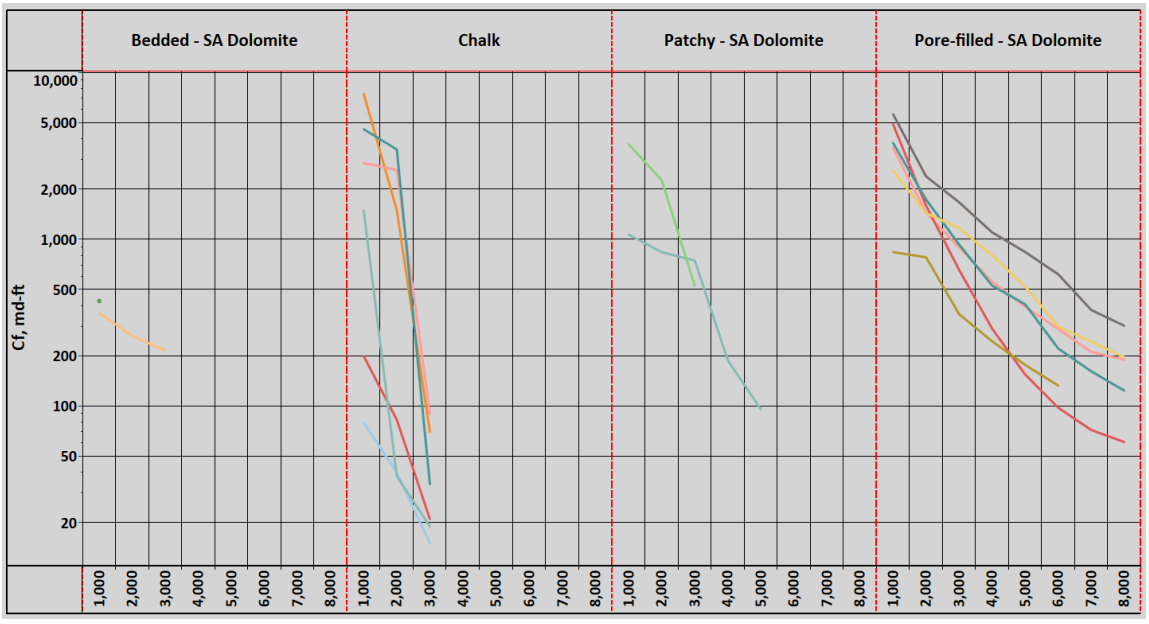

Figure 58 San Andres dolomite acid fracture conductivity comparison with chalk

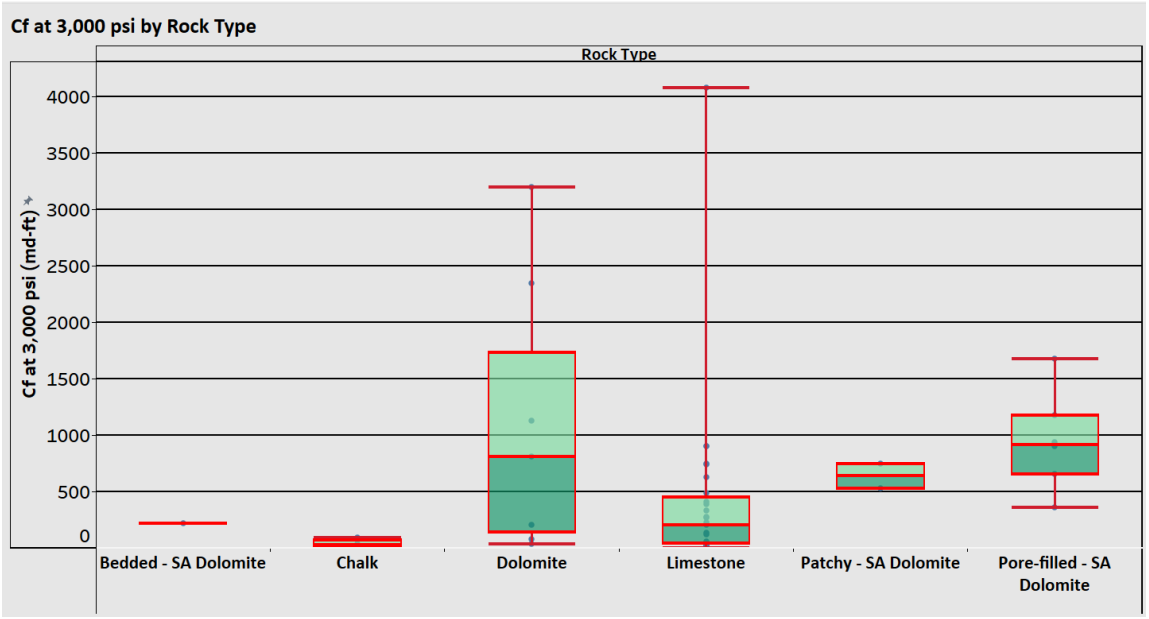

Figure 59 Summary acid fracture conductivity at 3,000 psi closure stress comparison with other rock types

4. CONCLUSIONS AND RECOMMENDATIONS

4.1. Conclusion

Based on the experimental results using San Andres dolomite rocks with high variations of anhydrite content from 1% to 43%, which were acidized using 15% HCl, 1,000 psi cell pressure, 1 L/ minute injection rate, 130 ºF cell temperature, and 10-minute injection, and measuring its acid fracture conductivity at closure stresses from 1,000 psi to 8,000 psi, the following conclusions were drawn as follows:

1. Surface characterization of San Andres dolomite sample cores was characterized using Lucia et al classification of anhydrite distribution.
2. There are poor correlations on acid etched volume vs percentage mineralogy, acid fracture conductivity vs acid etched volume, and acid fracture conductivity vs percentage mineralogy if there is high amount, which is greater than 2% content, of minerals other than anhydrite and dolomite, such as quartz, clay (kaolinite, illite, and chlorite), and oligoclase feldspar.
3. Good correlation on acid etched volume vs percentage mineralogy, acid fracture conductivity vs acid etched volume, and acid fracture conductivity vs percentage mineralogy could only be achieved if the samples, which have non-anhydrite and dolomite greater than 2%, were removed from the analysis.
4. Based on good correlations, acid etched volume and acid fracture conductivity are proportional to percentage of dolomite and both parameters are inversely

proportional to percentage of anhydrite. Besides, acid fracture conductivity is proportional to acid etched volume.

5. Acid fracture conductivity decline rate could be categorized based on anhydrite distribution on the fracture surfaces.
6. Bedded anhydrite distribution has the lowest acid fracture conductivity at zero closure stress (400 – 650 md-ft) and 3,000 psi (216 md-ft), but it has the lowest decline rate of acid fracture conductivity ($3 \times 10^{-4}\ psi$).
7. The lowest value of acid fracture conductivity on bedded anhydrite distribution is probably caused by the presence of anhydrite that is perpendicular to the fluid flow caused additional restriction for fluid to flow.
8. The perpendicular to the flow is caused by coring process on the vertical well that position the bedded anhydrite to the perpendicular to the flow in the experiment. However, in the reservoir, this bedded anhydrite is parallel to the fluid flow and will not cause the additional restriction that prevents the fluid to flow.
9. Patchy distribution has higher and wider range of acid fracture conductivity at zero closure stress, which were from 2,500 md-ft to 12,000 md-ft. Besides, it has higher acid fracture conductivity decline rate, which were from 6×10^{-4} psi to 10×10^{-4} psi, and higher value of acid fracture conductivity at 3,000 psi, which were from 350 md-ft to 750 md-ft.
10. Pore-filled distribution has lower and narrower range of acid fracture conductivity, which were from 1,350 md-ft to 6,150 md-ft, than patchy

distribution but higher than bedded anhydrite. Besides, it also has lower acid fracture conductivity decline rate, which were from 4×10^{-4} psi to 5×10^{-4} psi, and highest and widest value of acid fracture conductivity at 3,000 psi, which were from 350 md-ft to 1,650 md-ft.

11. San Andres dolomite with anhydrite distribution on the fracture surfaces has better value of acid fracture conductivity than chalk and limestone.

4.2. Lessons Learned and Recommendations

Based on the experimental works completed in the study, there are some lessons learned and recommendations to improve our understanding on the effect of anhydrite on the fracture surfaces of San Andres dolomite sample cores, which are as follows:

1. Rough surface of core sample has three difficulties observed in the experiment. First, when splitting the sample core into halves, there is possibility that the result of breaking sample into halves has highly angled core sample which presents difficulties in preparing the core sample and making sure that all sides of core sample were completely covered with silicone sealant. Second, the existing x-ray fluorescence (XRF) in the university cannot measure and identify elemental mineralogy on the highly steep area of rough surface. This is the reason why we did not use XRF in this study. Third, highly angle of core sample presents difficulties in positioning two fracture surfaces in the middle of designated-hole for pressure transducers and inlet-outlet injection and conductivity cell. This condition may lead to erroneous results of pressure

reading during acid fracture conductivity measurement leading to unreasonable acid fracture conductivity value.

2. The next experimental works may use smooth surface of core sample because it is easier to make a sample and make sure that all sides of core sample are completely covered with silicone-sealant. It also allows us to measure XRF for the whole fracture surfaces to obtain elemental distribution of mineralogy on the fracture surface that will improve our understanding on heterogeneity and its acid etched profile. Lastly, it is easier to position in the middle of designated hole of acid and conductivity cell to get accurate pressure reading.
3. Need more experimental results on patchy distribution and bedded anhydrite in order to have sufficient samples to draw conclusion.
4. One of the challenges on this study was having the same number of core samples of anhydrite distribution because we could not control the anhydrite distribution on the fracture surface. This was the reason why pore-filled anhydrite distribution has more samples than patchy and bedded anhydrite distribution.
5. Need to have experimental works with higher concentration of regular acid such as 20% HCl in order to see how significant the effect of acid concentration to acid fracture conductivity on dolomite with anhydrite distribution.
6. Need to do triaxial test and rock embedment test to measure young modulus and rock embedment strength on each mineral in sample cores to have better

understanding of the effect of elastic properties of rocks and rock embedment strength to acid fracture conductivity.

REFERENCES

Abass, H.H., Al-Mulhem, A.A., and Mirajuddin, K.R. 2006. Acid Fracturing or Proppant Fracturing in Carbonate Formation? A Rock Mechanic's View. Paper SPE 102590 presented at the SPE Annual Technical Conference and Exhibition, San Antonio, Texas, 24-27 September.

Akbar, M., Petricola, M., Watfa, M., Badri, M., Charara, M., Boyd A., Cassell B., Nurmi R., Delhomme J.P., Grace M., Kenyon B., Roestenburg J. 1995. Classic Interpretation Problems: Evaluating Carbonates. Schlumberger Oilfield Review, January 1995.

Akbar, M., Vissapragada, B., Alghamdi, A.H., Allen D., Herron M., Carnegie A., Dutta D., Olesen J.R., Chourasiya R.D., Logan D., Stief D., Netherwood R., Russel S.D., Saxena K. 2000. A Snapshot of Carbonate Reservoir Evaluation. Schlumberger Oilfield Review, Winter 2000/2001.

Almomen, A. M. A. 2013. The Effects of Initial Condition of Fracture Surfaces, Acid Spending, and Type on Conductivity of Acid Fracture. M.S. Thesis, Texas A&M University, College Station, Texas (August 2013).

Anderson, M.S., and Fredrickson, S.E. 1989. Dynamic Etching Tests Aid Fracture-Acidizing Treatment Design. SPE Production Engineering 4 (4): 443-449. SPE 16452.
Barron, A. N., Hendrickson, A. R., Wieland, D. R. et. 1962. The Effect of Flow on Acid Reactivity in a Carbonate Fracture. J. Pet Tech. 14 (4):443.-449. SPE-134.

Bartko, K.M., Conway, M.W., Krawietz, T.E. et al. 1992. Field and Laboratory Experience in Closed Fracture Acidizing the Lisburne Field, Prudhoe Bay, Alaska. Presented at the SPE Annual Technical Conference and Exhibition, Washington, DC, 4-7 October. SPE-24855-MS.

Beg, M.S., Kunak, A.O., Gong, M. et al. 1998. A Systematic Experimental Study of Acid Fracture Conductivity. *SPE Prod & Fac* **13** (4): 267-271. SPE-52402-PA.

Broaddus, G.C., Knox, J.A. and Fredrickson, S.E. 1968. Dynamic Etching Tests and Their Use in Planning Acid Treatments. Paper SPE 2362 presented at the Oklahoma Regional Meeting of the Society of Petroleum Engineers of AIME, Stillwater, Oklahoma, 25 October.

Deng, J., Mou, Jianye., Hill, A. D. et al. 2012. A New Correlation of Acid-Fracture Conductivity Subject to Closure Stress. SPE Production & Operation 27 (2). 158-169. SPE-140402.

Economides, M.J., Hill, A.D., and Ehlig-Economides, C. 1994. Petroleum Production Systems. New Jersey: Prentice Hall Petroleum Engineering Series.

E.R. Crain. 1999. Crain's Petrophysical Handbook. www.spec2000.net**.**

Gong, M., Lacote, S., and Hill, A.D. 1998. New Model of Acid-Fracture Conductivity Based on Deformation of Surface Asperities. Paper SPE 39431 presented at the SPE International Formation Damage Symposium, Lafayette, Louisiana, 18-19 February.

James, N.P., Jones, B. 2016. *Origin of Carbonate Sedimentary Rocks.* West Sussex: John Wiley & Sons.

Jin, X., Zhu, D., Hill, A. D., & McDuff, D. 2019. Effects of Heterogeneity in Mineralogy Distribution on Acid Fracturing Efficiency. Paper SPE 194377 presented at SPE Hydraulic Fracturing Technology Conference and Exhibition, The Woodlands, Texas, 5 – 7 February.

Lucia, F.J. 1999. *Carbonate Reservoir Characterization.* Berlin: Springer – Verlag.
Lund, K., Fogler, H.S., and McCune, C.C. 1973. Acidizing-I. The Dissolution of Dalcite in Hydrochloric Acid, Chemical Engineering Science 28, 691-700.

Lund, K., Fogler, H.S., McCune, C.C., and Ault, J.W. 1975. Acidizing-II. The Dissolution of Calcite in Hydrochloric Acid, Chemical Engineering Science 30, 825-835.

Malagon, C. 2006. The Texture of Acidized Fracture Surfaces-Implications for Acid Fracture Conductivity. MS thesis, Texas A&M University, College Station, Texas (May 2006).

Malik, M. A. and Hill, A. D. 1989. A New Technique for Laboratory Measurement of Acid Fracture Conductivity. Paper SPE 19733 presented at the SPE Annual Technical Conference and Exhibition, San Antonio, Texas, 8-11 October.

Melendez, M.G. 2007. The Effects of Acid Contact Time and Rock Surfaces on Acid Fracture Conductivity. MS thesis, Texas A&M University, College Station, Texas (August 2007).

Neumann, L. F., Oliveira, T. J. L., and Fernandes, P. D. a.2012. Building Acid Frac Conductivity in Highly-Confined Carbonates. Paper SPE 152164 presented at the SPE Hydraulic Fracturing Technology Conference, The Woodlands, Texas, 6-8 February.

Neumann, L. F., de Oliveira e Sousa, J. L. A. O., and Oliveira, T. J. L. b.2012. Acid Fracturing: New Insigths on Acid Etching Patterns from Experimental Investigation. Paper SPE 152179 presented at the SPE Hydraulic Fracturing Technology Conference, The Woodlands, Texas, 6-8 February.

Nierode, D.E., and Kruk, K.F. 1973. An Evaluation of Acid Fluid Loss Additives, Retarded Acids, and Acidized Fracture Conductivity. Paper SPE 4549 presented at the Annual Fall Meeting, Las Vegas, Nevada, 30 September–3 October.

Nierode, D. E., Williams, B. R. and Bombardieri, C. C. 1972. Prediction of Stimulation from Acid Fracturing Treatments. Journal of Canadian Petroleum Technology 11 (4). 31-41. SPE-72-04-04.

Penaloza, A.N. 2013. Experimental Study of Acid Fracture Conductivity of Austin Chalk Formation. M.S. Thesis, Texas A&M University, College Station, Texas (May 2013).

Pournik, M. 2008. Laboratory-Scale Fracture Conductivity Created by Acid Etching. PhD dissertation, Texas A&M University, College Station, Texas (December 2008).

Roehl, P.O., Choquette, P.W. 1985. *Carbonate Petroleum Reservoirs.* New York: Springer – Verlag.

Suleimenova, A. 2015. Acid Fracturing Feasibility Study for Heterogeneous Carbonate Formation. M.S. Thesis, Texas A&M University, College Station, Texas (May 2015).

Taylor, K.C., Alghamdi, A.H., Nasreldin, H.A. 2004. Effect of Additives on the Acid Dissolution Rates of Calcium and Magnesium Carbonates, paper SPE 80256 presented at the 2003 SPE International Symposium on Oilfield Chemistry, Houston, Texas, 5 – 6 February.

Underwood, J. T. 2013. Acid Fracture and Fracture Conductivity Study of Field Rock Samples. M.S. Thesis, Texas A&M University, College Station, Texas (December 2013).

Van Domelen, M.S. 1992. Optimizing Fracture Acidizing Treatment Design by Integrating Core Testing, Field Testing, and Computer Simulation. Paper SPE 22393 presented at the SPE International Meeting on Petroleum Engineering, Beijing, China, 24-27 March.

Van Domelen, M.S., Gdanski, R.D., Finley, D.B. 1994. The Application of Core and Well Testing to Fracture Acidizing Treatment Design: A Case Study. Paper SPE 27621 presented at the European Production Operations Conference and Exhibition, Aberdeen, U.K., 15-17 March.

Wang, X. 2015. Acid Fracture and Fracture Conductivity Study on Heterogeneous Carbonate Rock Samples. M.S. Thesis, Texas A&M University, College Station, Texas (December 2015).

Zou, C.L. 2006. Development and Testing of an Advanced Acid Fracture Conductivity Apparatus. M.S. Thesis, Texas A&M University, College Station, Texas (2006).

APPENDIX A

SURFACE SCAN PROFILOMETER RESULTS

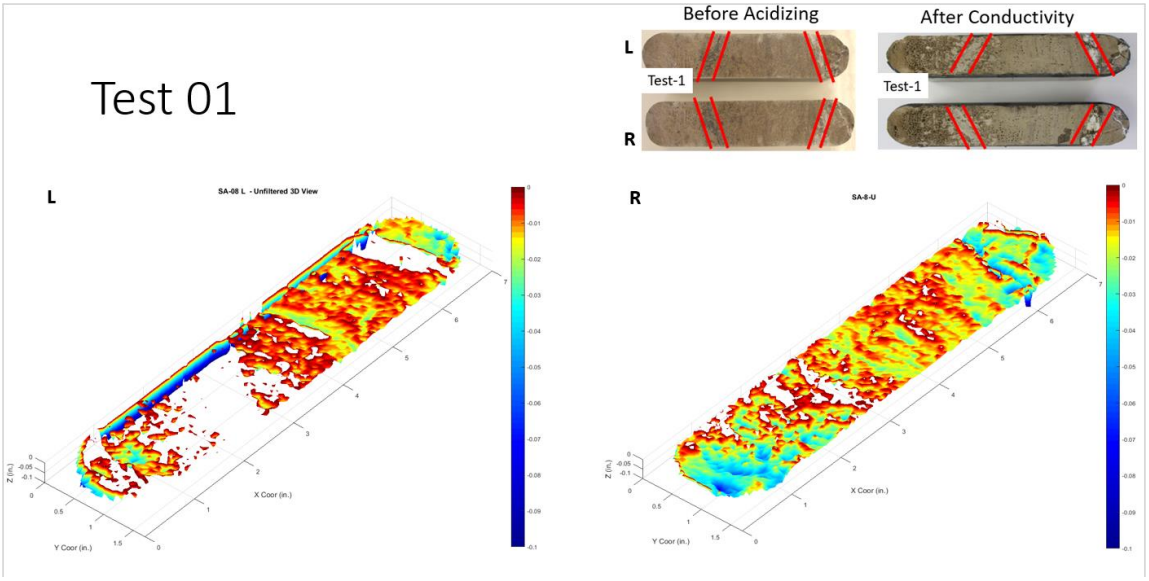

Figure A- 1 Acid etched profile of test 01

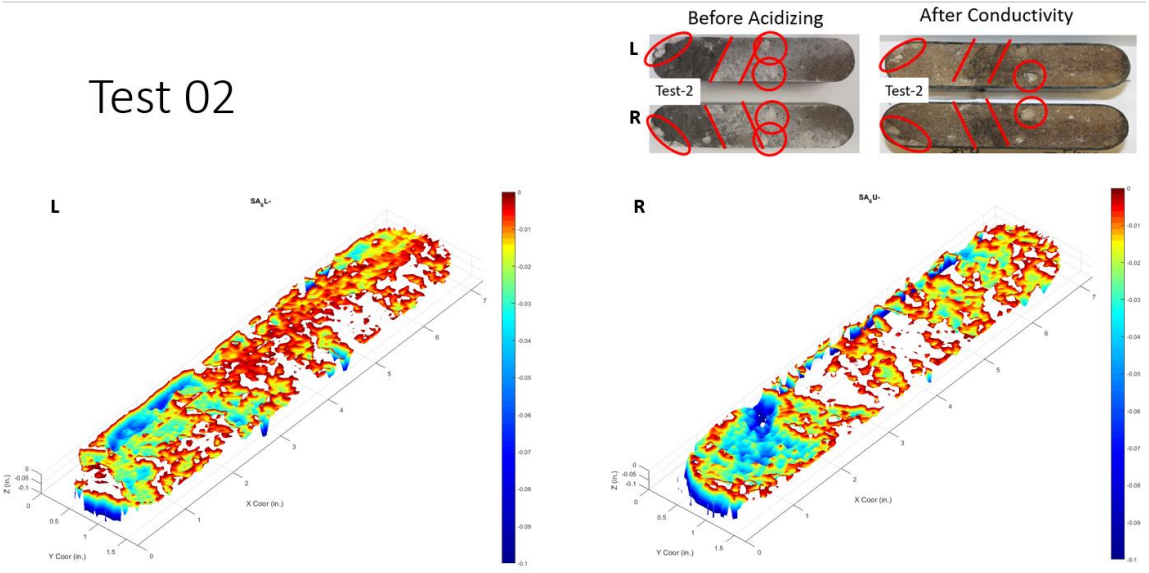

Figure A- 2 Acid etched profile of test 02

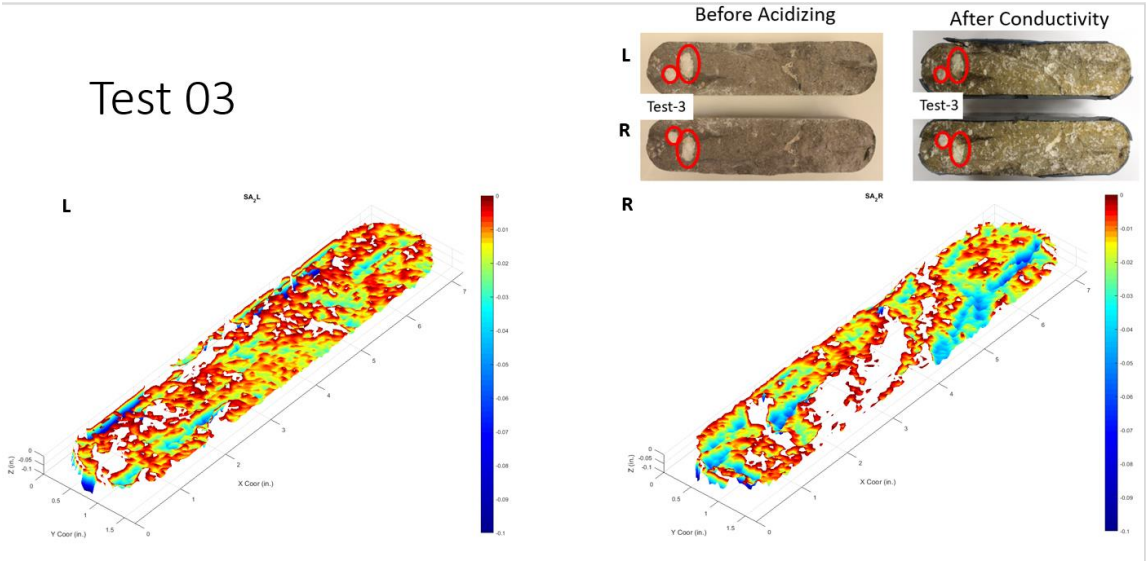

Figure A- 3 Acid etched profile of test 03

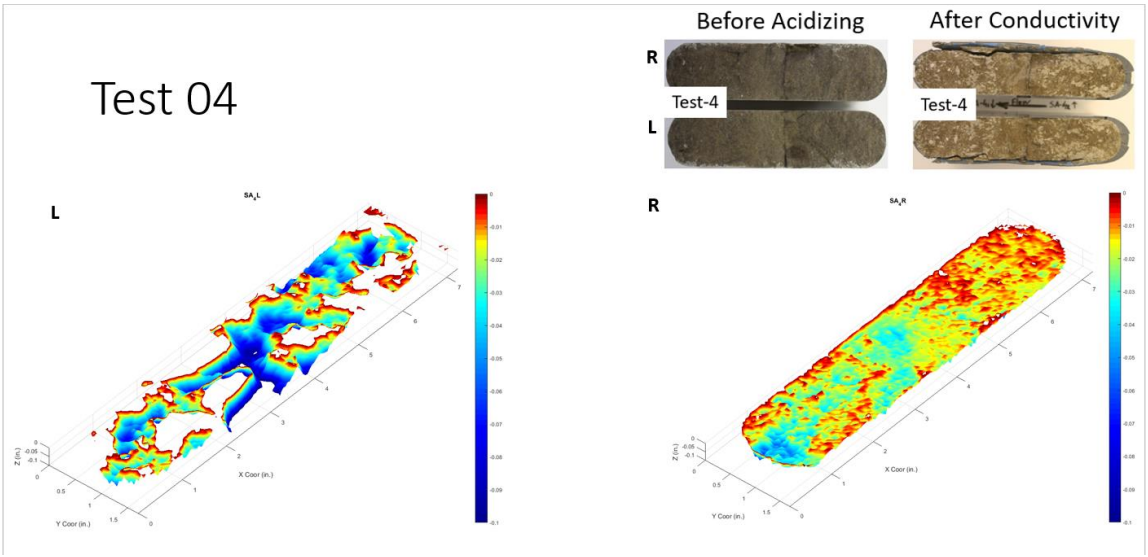

Figure A- 4 Acid etched profile of test 04

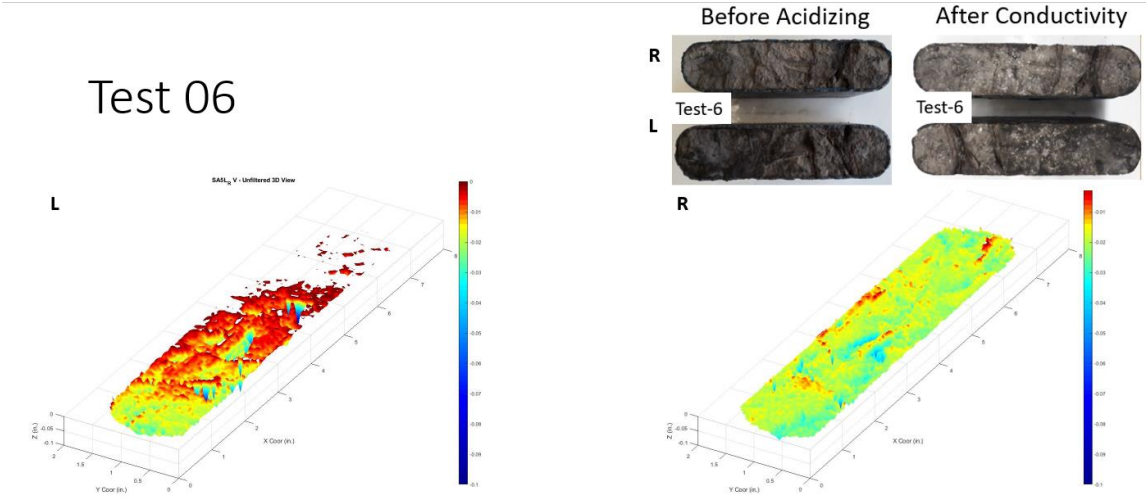

Figure A- 5 Acid etched profile of test 06

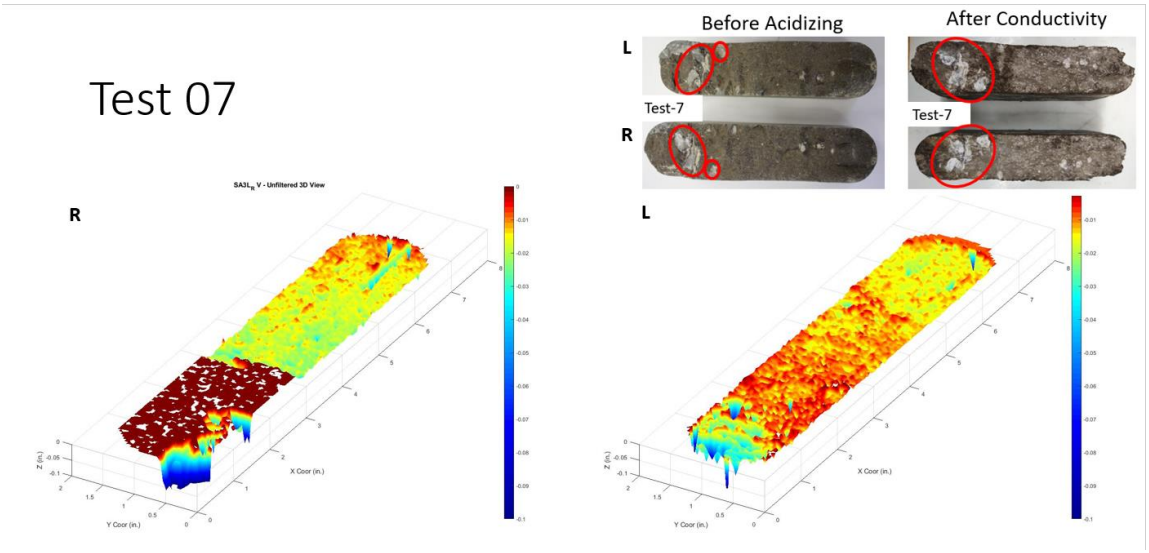

Figure A- 6 Acid etched profile of test 07

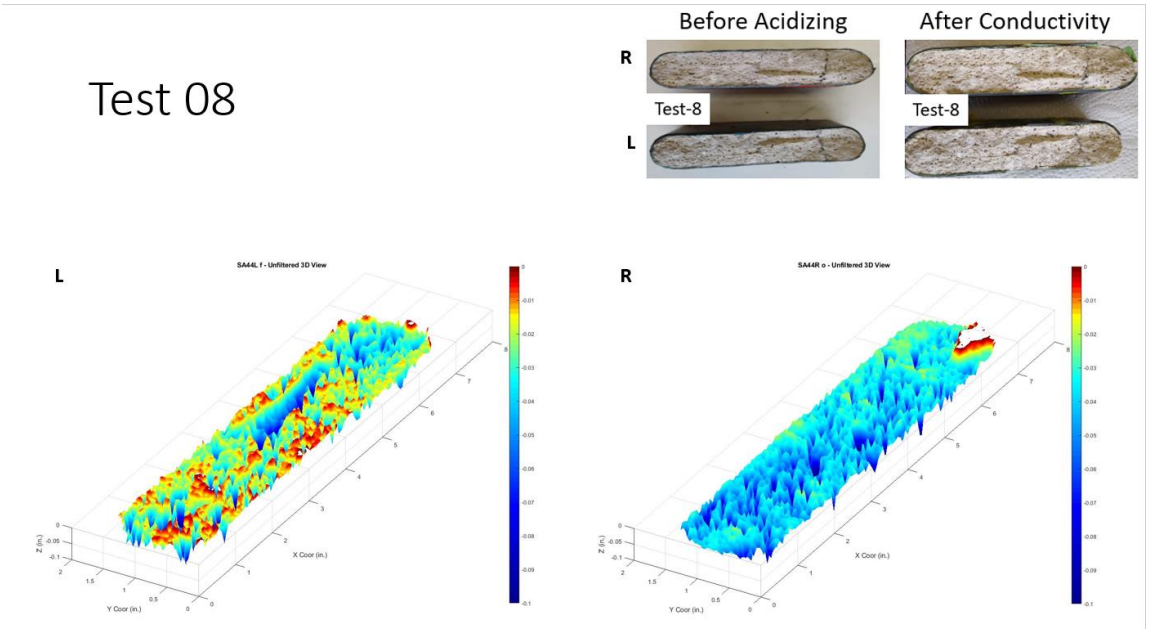

Figure A- 7 Acid etched profile of test 08

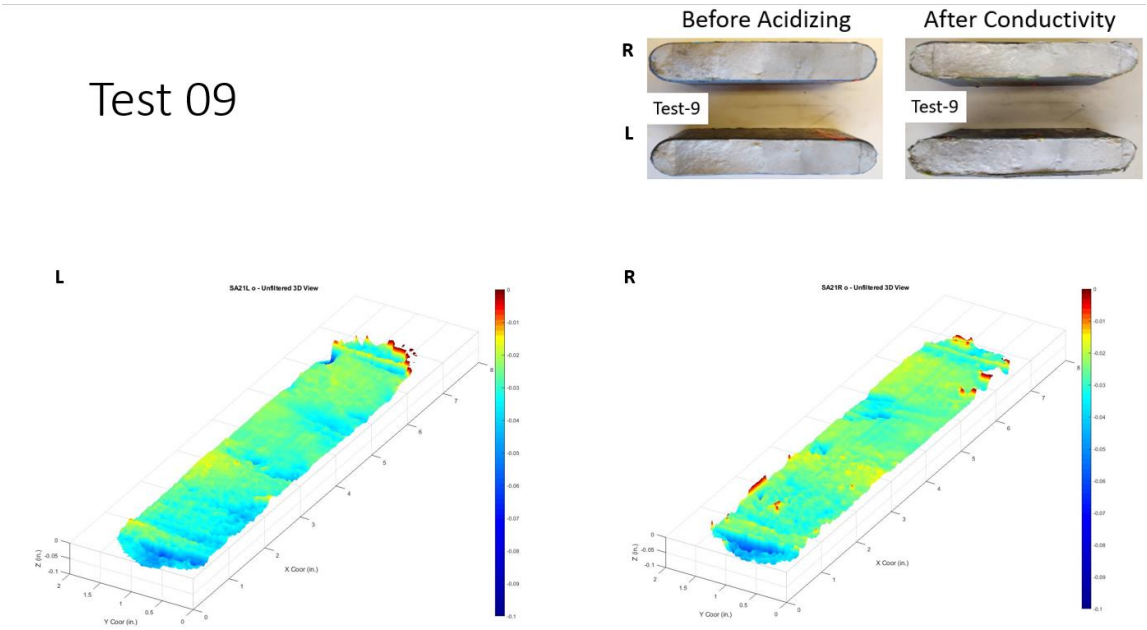

Figure A- 8 Acid etched profile of test 09

Test 10

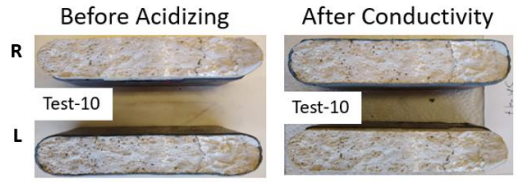

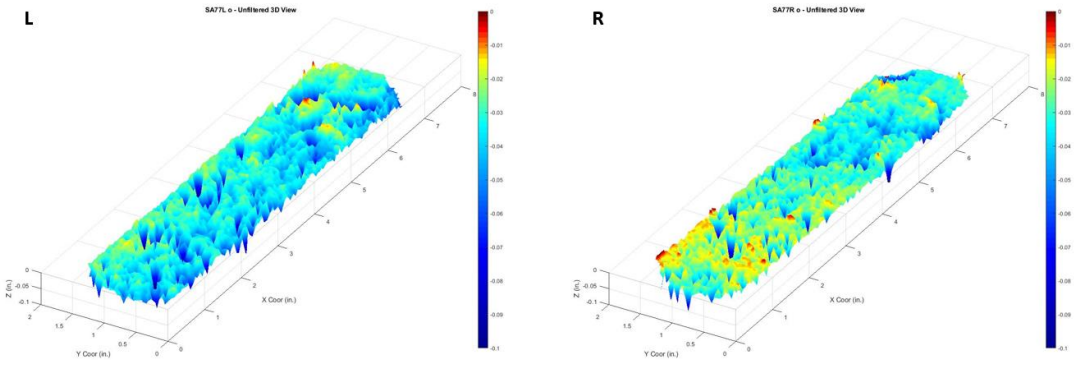

Figure A- 9 Acid etched profile of test 10

Test 11

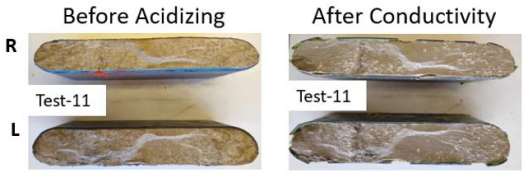

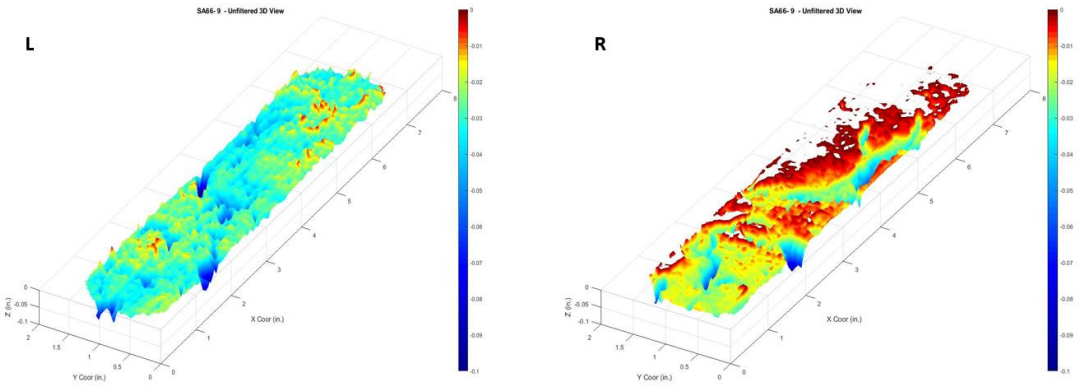

Figure A- 10 Acid etched profile of test 11

Test 12

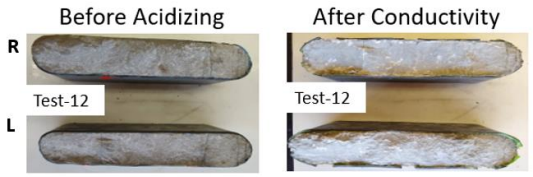

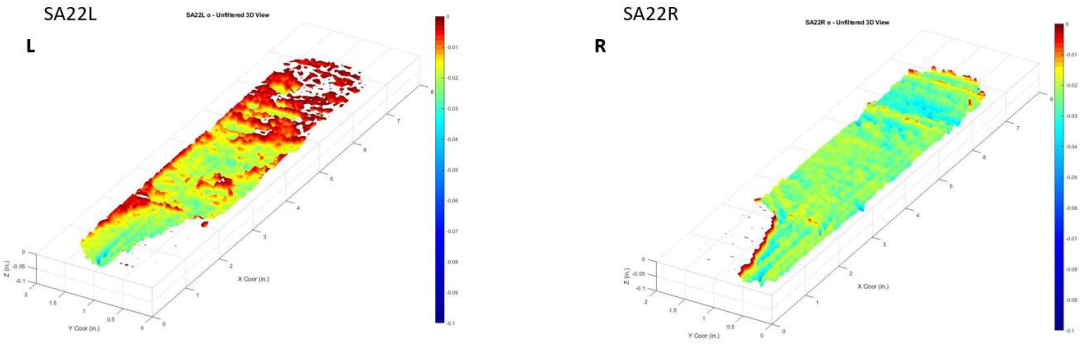

Figure A- 11 Acid etched profile of test 12

APPENDIX B

CONSTANTS USED TO CALCULATE FRACTURE CONDUCTIVITY

N2 Molecular Weight (MW) [kg/mol]	M	0.0280134
Fracture Width (h_f) [in]	h	1.75
Z factor (Z)	Z factor	1
(R) [J/mol K]	R	8.3144
Temp (T) [F]	T	73.4
Temp (T) [K]	T	293.15
Fracture Length (L) [in]	L	5.25
N2 Viscosity (μ) [Pa*s]	μ	1.75923E-05
N2 Density (ρ_f) [kg/m^3]	ρ	1.16085